Geological 3D-modeling of the Virtasalmi Cu deposit in eastern Finland

LAURI TAPIO VIRNES

MASTER'S THESIS

OULU MINING SCHOOL

UNIVERSITY OF OULU

2018

Abstract

Modern computing power and advanced 3D-modeling software have made the modeling of geological, geophysical, geochemical and structural data a widely used method in active mine production as well as in brownfield exploration, where it can be used for visualization, planning and target generation. In this study, the Paleoproterozoic Cu-dominated VMS deposit of Virtasalmi and related mine were modeled to produce the first modern 3D-model of the deposit and to test the accuracy of the digitized historical datasets. A total of 239 drill holes from the Virtasalmi mine area were used, from which the collar locations, downhole surveys, lithological logs and geochemical assays were digitized and added to a geological database. Around 3000 Cu analyses were utilized for modeling of the general low-grade (0.2–0.7 wt.% Cu) and high-grade (>0.7 wt.% Cu) mineralization solids. The results show that before the mining operations were started, the Virtasalmi deposit consisted of several high-aspect-ratio lenses, which had a combined strike length of ~626 m near the surface and extended up to ~344 meters below the surface. The performed unofficial resource estimation indicates that the area contained a total of 4.83 Mt of mineralized material, of which ~3.51 Mt was low-grade mineralization and 1.32 Mt high-grade mineralization. Based on the model, roughly 500 000 tons of mineralized material is still left unmined in the Virtasalmi mine area.

Keywords: 3D-modelling, Resource estimation, Virtasalmi Mine, VMS deposits.

Contents

1. Introduction

Within the past couple of decades, 3D-modeling of geological, geophysical, geochemical and structural data in both greenfield and brownfield exploration has become a household discipline for many researchers, and exploration and mining companies. Understanding the complexity of the geology in a mining district has been shown to lead to the extension of life-of-mine of operating mines and discoveries of continuations of ore-bearing horizons in the subsurface or even new, prospective areas (e.g., Fan et al. 2017, Li et al. 2015, Jansson et al. 2013, Martin et al. 2007).

The Cu-bearing stratabound, polydeformed and metamorphosed volcanogenic massive sulfide deposit (VMS) of Virtasalmi is located close to the Virtasalmi town in the municipality of Pieksänmäki in eastern Finland. Historically, the deposit has also been called the Hällinmäki deposit or Karsikumpu deposit. The mineralization was exploited by Outokumpu Oy between 1966 and 1984 in two stages, which included open pit mining and underground operations. A total of ~4.2 Mt of Cu ore was extracted during these mining operations (Puustinen 2003). After the initial exploration drilling by GTK, Hyvärinen (1966, 1969) presented a comprehensive geological description, a model for ore genesis as well as an initial resource estimate. Later Lawrie (1988, 1992) conducted a structural and geochemical study of the Virtasalmi district and defined the Virtasalmi mineralization as a VMS deposit. Since Lawrie's investigations, no comprehensive studies of the Virtasalmi amphibolites have been undertaken. During the operation of the Virtasalmi mine, near-mine exploration for ore lenses at greater depth was generally minor and unsuccessful.

The purpose of this thesis was to collect, digitize and exploit historical data from the Virtasalmi mine in modern modeling software in order to reconstruct the pre-mining extent of the mineralization by generating a 3D-model of the Cu mineralization. The work was conducted using GEOVIA Surpac 6.7.2 for 3D-modeling and ESRI ArcMap 10.3 for map digitization and georeferencing. The data utilized come from 239 diamond drill holes which were drilled and analyzed for copper during the exploration and operation of the mine. The model presented here can act as a starting point for further research or exploration and can be useful for resource classification in a system like

UNFC (United Nations Framework Classification for Resources). The aim is also to explore the accuracy and validity of a model generated from the historical data.

2. Volcanogenic massive sulfide deposits

Volcanogenic massive sulfide deposits (VMS), also called volcanic-hosted massive sulfide deposits (VHMS) are a major source of base metals, such as Cu, Zn and Pb. Additionally, precious metals Au and Ag are a common side product obtained from VMS deposits (Koski and Moiser 2012, Shanks and Koski 2012, Pirajno 2008, Galley et al. 2007). Globally around 1100 VMS deposits are currently known. More than 800 of these deposits are of a significant size, containing sulfide ore from 200 Kt to more than 150 Mt (Koski and Moiser 2012, Galley et al. 2007). Age-wise, the VMS deposits range from modern active systems to early Archean deposits. However, there are time periods in the geological record when the formation of VMS deposits was especially active, including ~2.76 Ga, ~1.96 Ga, 0.6-0.25 Ga and 0.03 Ga. These times are temporally associated with ocean closing phases in the supercontinent cycle (Cawood and Hawkesworth, 2013, Koski and Moiser 2012, Bradley 2011). Preservation bias towards back arc-related VMS deposits means that many of the known VMS deposits are connected to periods of major ocean closing and deposits tend to be found near continental margins or in a proximity to suture zones (Cawood and Hawkesworth 2013, Galley et al. 2007, Groves et al. 2005).

VMS deposits form near or directly on the sea floor as stratabound, sometimes exhalative, mineralization when acidic metal-bearing hydrothermal fluids are subjected to changes in pressure, temperature, oxidation or pH (Pirajno 2008, Huston and Large 1989). The change in these conditions induces the precipitation of various sulfides, sulfates, calcite, amorphous silica, quartz and Fe oxides. Usually the most abundant sulfide species are iron sulfides, such as pyrite, pyrrhotite and marcasite. In economic deposits, the Fe sulfides are accompanied by sphalerite, chalcopyrite and sometimes galena (Shanks and Koski 2012, Koski and Moiser 2012, Pirajno 2008, Peter et al. 1988).

Formation of VMS deposits generally takes place in mid-ocean spreading centers and back-arc spreading basins, which are dominantly extensional tectonic settings. However, VMS deposits are likely to occur anywhere with submarine volcanism, and

thus probable tectonic environments include also subduction-related, intra-oceanic and continental margin magmatic arcs (Shanks and Koski 2012, Huston et al. 2010, Pirajno 2008, Van Kranendonk et al. 2006a, Kerrich et al. 2005). High thermal input of volcanically active areas in combination with crustal extension are important factors for VMS formation. In these tectonic environments, high heat flow provides the necessary energy for driving hydrothermal fluid circulation and extension-related faulting and fracturing provide channel ways for concentrated fluid movement and discharge (Pirajno 2008, Galley et al. 2007).

An idealized example of a VMS deposit consists of a VMS mound structure, which is situated on the sea floor at a depth of more than 1000 meters. The mound can be tens of meters high and hundreds of meters long and wide. This main mound can show additional relief formed of smaller mounds (Thompson et al. 1988). The main mound can be formed from a combination of fragmented country rocks with blocks and pieces of massive sulfide material. The smaller, additional mounds are made of fragments of sulfide material and indicate locations of vigorous exhalation of hydrothermal fluids. Depending on the environment, features between active smaller vent mounds can be covered by metalliferous sediments (Herzing and Hannington 1995, Thompson et al. 1988). The venting or exhalation of hydrothermal fluids takes place from chimney structures and cones forming on top of the VMS mounds. These chimneys can be either high-temperature, sulfide-venting black smokers (over 350 °C) or cooler, barite-, silica- and sphalerite-venting, white smokers (100–350 °C) (Pirajno 2008, Humphris et al. 1995b, Herzing and Hannington 1995). Normally black smokers form in the inner parts of a VMS mound while the white smokers occupy distal parts of the system. Precipitation of sulfides and additional gangue material takes place in the vent zones immediately at contact with the cool seawater. Minerals add material to the growth of the existing chimneys or they are dispersed in the water column in a cloud and proceed to fall on the sea floor in the proximity of the chimney structures (Pirajno 2008, Herzing and Hannington 1995, Thompson et al. 1988).

Underneath the VMS mounds, footwall lithologies can consists of a variety of volcanic rocks and sedimentary units, both which are dependent on the overall tectonic setting of the area. In an idealized example, the footwall rocks are the host to a discordant, subvertical, pipe- or carrot-shaped alteration zone, which can be several hundreds of meters deep (Hannington et al. 1998). However, deposits where fluids have moved

laterally in permeable horizons do not exhibit these discordant alteration zones (Raymond 1996). The alteration zone consists of a fractured and pervasively altered country rocks and is commonly called a feeder or stringer zone. The feeder zone signifies an area of concentrated hydrothermal fluid ascension before the fluids are vented on the sea floor (Shanks and Koski 2012, Pirajno 2008, Hannington et al. 1998, Herzing and Hannington 1995). The alteration mineral assemblage present in and around the feeder zone and the alteration intensity are controlled by temperature, pH, fluid/rock ratio and activity of cations (Mg, Ca, Na) (Pisutha-Arnond and Ohmoto 1983). Normally, heat flow and F/R ratio are high and alteration strong beneath the VMS mounds. The intensity of alteration decreases with distance to the mound. The central part is altered by strong silification and have a mineral assemblage of sericite + chlorite + quartz ± clays. More distal parts of the system are less serisitic and chloritic with montomorillonite and zeolites taking their place. Common components of the feeder zones are also chalcopyrite and quartz veins and disseminated Cu-rich sulfide mineralization (Shanks and Koski 2012, Bonnet and Corriveau 2007, Herzing and Hannington 1995).

Thermal gradient not only contributes to the intensity and type of alteration surrounding a VMS mineralization, but it also effects the metal zonation exhibited by many VMS deposits. Metal zonation is formed during the gradual growth of the VMS mound when additional sulfide mass insulates the inner zones of the mound and low temperature sulfides, such as sphalerite and marcasite, migrate towards the outer shell of the mound while they are being replaced by high-temperature sulfide species including chalcopyrite, cubanite, bornite and pyrrhotite. For this reason, the sulfide mineralization in a VMS feeder zone is dominated by Cu sulfides (Shanks and Koski 2012, Pirajno 2008).

The metals enriched in VMS deposits are mostly scavenged from the oceanic lithosphere that surround the deposit. Copper, Zn and Fe are derived from mafic or ultramafic country rocks. A VMS system with a significant amount of Pb requires a Pb source, such as sedimentary units or felsic volcanic rocks (Rona 1984). Additional metals to the VMS forming hydrothermal fluids are contributed by magmatic fluids generated by magma degassing (Bonnet and Corriveau 2007, Yang and Scott 1996, Lydon 1988). This could especially be the case in fast spreading ridges, back-arc basins and suprasubduction-related VMS deposits since the heat-providing magma chambers

are relatively shallowly emplaced (Yang and Scott 1996, Pirajno 2008). The sulfur in the VMS systems is mostly derived by reduction of seawater sulfate while leaching of sulfides already present in the country rocks is also likely to contribute (Huston et al. 2001, Walshe and Solomon 1981, Solomon 1976).

While VMS deposits tend to be polymetallic ore formations, there is still a number of deposits, including Virtasalmi, where the mineralization consists mainly of Cu sulfides. A modern example exists on the Galapagos rift where venting hydrothermal fluids at 350–400 °C are creating Cu-dominated mineralization (Skirrow 1982). In the Solean graben in Cyprus, a late Cretaceous Cu-dominated hydrothermal convection system is part of the Troodos ophiolite. There a hydrothermal convection cell was active away from the major spreading axis. The Cu mineralization and the alteration of country rocks postdate the magmatism, faulting and deformation related to extension at the spreading ridge. An argillic altered feeder zone has been identified from the area. Underlying the feeder zone is an intensely hydrothermally metasomatized zone where original sheeted dikes have been altered into granular epidote-quartz-chlorite "epidosites" (Schiffman et al. 1987).

The Mt. Lyell mining field located on the Tasmanian west coast near Queenstown is a host to seventeen large VMS deposits, some of which are still being exploited (Raymond 1996). The Mt. Lyell area has a mixture of traditional VMS-type deposits and disseminated Cu-rich lenses hosted by hydrothermally altered middle Cambrian volcanic and volcanoclastic rocks (Perkins and Walshe 1993). The more typical VMS mineralization consists of massive pyrite-galena-sphalerite and pyrite-chalcopyrite mineralization lenses. Stratigraphically underlying the massive sulfide lenses are high-grade lenses containing disseminations and stringers of pyrite and chalcopyrite as well as zones with mainly bornite and chalcopyrite in them (Walshe and Solomon 1981). Some of these areas with a high Cu grade lack the traditional overlying massive sulfide mounds, and it is assumed that the original mounds have been eroded away (Corbett 2001).

An Archean example of the VMS system where the mineralization consists mainly of chalcopyrite and minor pyrrhotite has been reported from the ~3.7 Ga Isua supracrustal belt in western Greenland. In the Isua area, the disseminated, Cu-dominated mineralization is situated mainly in layered/banded tuffaceous amphibolites. The

mineralization has been interpreted to have an exhalative origin. It is associated with various iron formations, which also have been suggested to be related to the venting that created the disseminated Cu mineralization (Appel 1997).

3. Regional geology

The Virtasalmi area is located in the south-eastern corner of the Savo belt (Figs. 1 and 2). Geologically, the area is part of the supracrustal rocks of the Raahe-Ladoga zone, being situated near the Raahe-Ladoga suture, which separates the Svecofennian island arc complex (west) and the Karelian craton (east) (Fig. 1) (Korsman et al. 1997, Kärki et al. 1995). The eastern and northern parts of the Svecofennian island arc complex and especially the Raahe-Ladoga zone host several VMS deposits including those of the Vihanti-Pyhäsalmi area north of Virtasalmi (Fig. 2). North-east of Virtasalmi lies the allochtonous Outokumpu nappe complex, which is also characterized by the presence of various VMS deposits (Peltonen et al., 2008) (Figs. 1 and 2).

The supracrustal rocks of the Virtasalmi area are ~1.91-1.92 Ga in age (Pekkarinen 2002, Vaasjoki and Sakko 1988) and consist of metasediments, such as mica schists or gneisses, and variably banded amphibolites (Kähkönen 2005). The protoliths of the amphibolites have been submarine subalkaline mafic volcanic rocks of andesitic to basaltic composition (Pekkarinen 2002, Lawrie 1992, Lawrie 1988). At Virtasalmi, the Svecofennian intrusive rocks are represented by a gabbro-diorite-quartz-diorite-tonalite-trondhjemite suite, which comprises ~60% of the rocks in the area (Lawrie 1988).

The rocks in the Virtasalmi area have undergone two major peaks of metamorphism. During D1, granulite facies conditions prevailed. This was followed by incomplete retrogression under lower amphibolite facies conditions during D2 (Vaasjoki and Sakko 1988; Lawrie 1988). Deformation in the region is expressed by folds, ductile shearing and younger brittle and semi-brittle reactivation of older shear zones (Kärki et al. 1995).

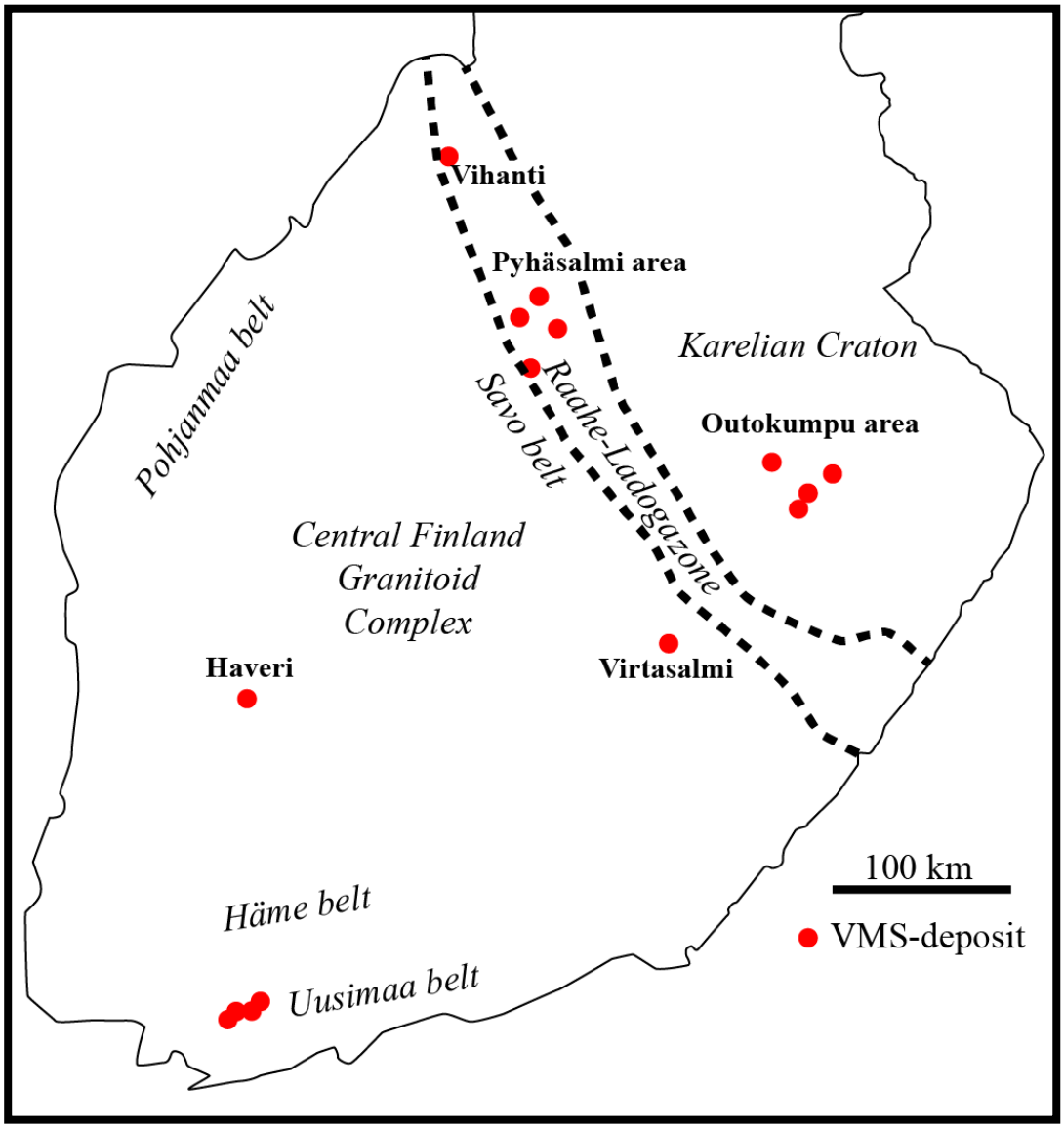

Fig. 1. Approximate distribution of major geological complexes in southern Finland and locations of major VMS deposits. Simplified after Hanski (2015).

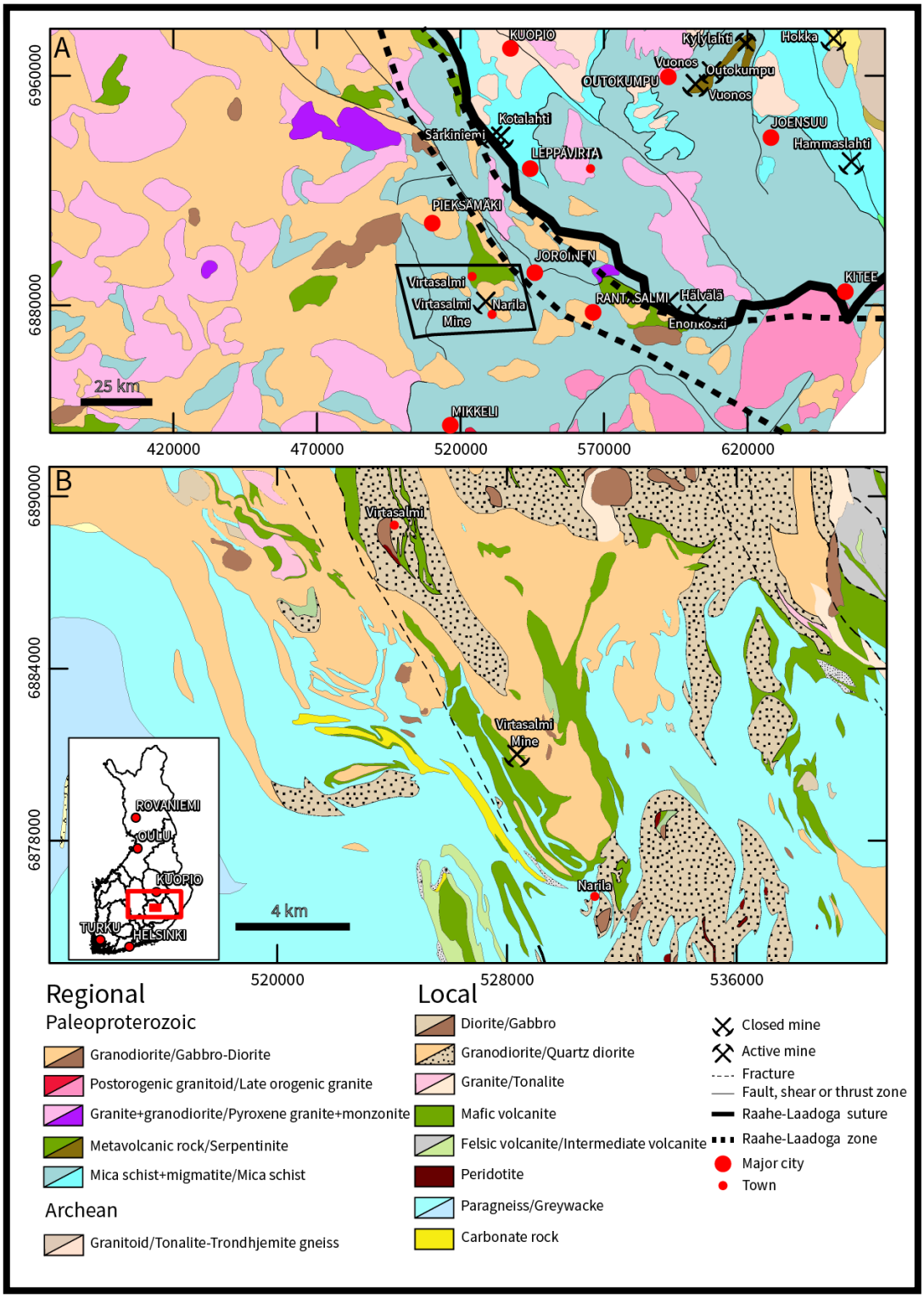

Fig. 2. A) Geological map of eastern Finland. B) Local geology of the Virtasalmi area. Based on maps Bedrock of Finland in scale 1:5 000 000 and Bedrock of Finland in scale 1:200 000 © Geological Survey of Finland

4. Geology of the Virtasalmi district

The Virtasalmi mineralization occurs in the Virtasalmi volcanic belt in the southern part of the Savo belt (SB), some 50 km north of the city of Mikkeli. The Savo belt runs roughly from Oulu to Joroinen and is roughly parallel to the NW-SE-trending Raahe-Ladoga suture zone (Figs. 1 and 2). In general, the supracrustal rocks of the Savo Belt consist of mica schists and migmatized gneisses. Locally, felsic and basaltic metavolcanites, now metamorphosed to quartz-feldspar schists and amphibolites, can be abundant (Kähkönen 2005, Lawrie 1992). Dating of the Virtasalmi belt is difficult because felsic metavolcanic rocks are missing in the rock sequence, but a U-Pb zircon age from a rhyolitic unit from a nearby locality at Joroinen (~30 km away) has yielded an age of 1906±4 Ma (Vaasjoki and Sakko 1988). This is somewhat younger than the age of metavolcanic rocks in the northern Savo Belt where a rhyolite from the Pyhäsalmi area has been dated at 1921±2 Ma (Kousa et al. 1994).

The most prevalent supracrustal rocks in the Virtasalmi area are fine-grained metasediments surrounding the Virtasalmi metavolcanic belt and carbonate rock units. The carbonate rocks range from thin interlayers to thicker lenticular units (Reinikainen 2001, Hyvärinen 1966). The supracrustal rocks of the Virtasalmi metavolcanic belt are amphibolites with skarns and minor carbonate rocks. Primary structures have been poorly preserved in the amphibolized metavolcanites but some local occurrences of pillow lavas, lava tubes, sills and dikes can be recognized (Lawrie 1988). As with the rest of the Svecofennian domain, the Virtasalmi belt has been dissected by pre-, syn- and late-kinematic intrusions (Kähkönen 2005, Kärki et al. 1995).

Lawrie (1992) describes three major and four local deformation phases in the Virtasalmi area. D1 folds have been overprinted but D1 fabrics have been preserved in rare localities. D2 and D3 features are preserved, with the deformation of these phases consisting of ductile deformational and upright and reclined folding. The four localized post-D3 deformational phases likewise formed upright folds and subvertical fabrics but these features are only local. Connected to the deformational phases, two major metamorphic peaks have affected the Virtasalmi area. The first peak (M1) took place under granulite fasies conditions, at 750-800 °C and 3.5-5.5 kbar. During D2, metamorphic peak M2 affected the rocks under lower amphibolite facies conditions, at 450-550 °C and 2-3.5 kbar. M2 caused retrogression and amphibolization of the

previous granulite mineral assemblages but this process was only partial and resulted in polymetamorphic mineral assemblages (Lawrie 1988).

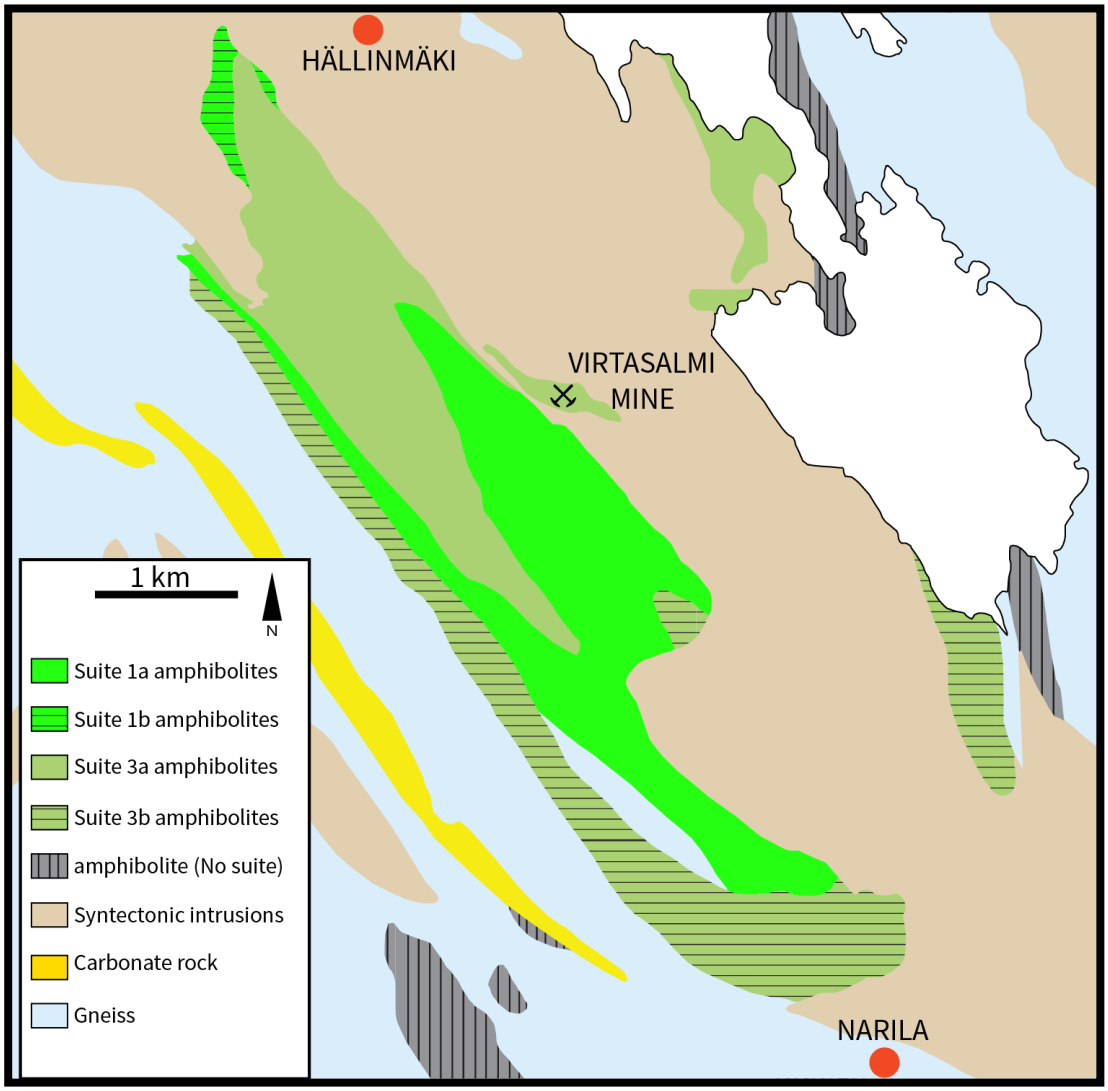

Fig. 3. Distribution of amphibolites near the Virtasalmi mine. Modified after Lawrie (1992).

4.1 Amphibolites

Some primary features, such as pillow lavas and lava tubes, have survived locally in low-strain zones. They indicate a submarine volcanic origin of the Virtasalmi amphibolites (Lawrie 1988). The stratigraphy or thickness of the volcanic pile has not been established mostly due to the wide distribution of intrusive lithologies in the area (Hyvärinen 1966, Lawrie 1988). Based on geochemistry, petrological differences and field relationships, Lawrie (1988) recognized four main suites and several subsuites of amphibolites in the Virtasalmi metavolcanic belt. All suites plot mostly in the tholeiitic

field in the Jensen cation plot (Fig. 4). All suites show low Zr/Nb and Y/Nb ratios. They also exhibit enrichment in light rare earth element (LREE), large-ion lithophile elements (LILE) and Nb relative to N-MORB. These features are most akin to within-plate basalts or E-MORB. Lawrie (1992) suggests an intra-cratonic or a passive continental margin setting for the Virtasalmi amphibolites.

The amphibolites hosting the ore body at the Virtasalmi mine are part of the suite 3. A summary of the most salient features after Lawrie (1988, 1992) is given below. Figure 3 illustrates the general distribution of amphibolitic rocks around the mine.

4.1.1 Suite 3 amphibolites

Suite 3 amphibolites are fine-grained, greenish black rocks consisting of clinopyroxene, hornblende, andesine-labradorite and titanite. The rocks of this suite are the host rocks for the disseminated Cu mineralization at Virtasalmi and they are often skarn-altered to varying degree or interlayered with skarn rocks. The suite has been divided into 3 subgroups (a-c). Geochemically, suite 3 is separated from suites 1 and 2 by its relatively low Y/Nd ratio, higher Zr/Y ratio and high Nb content. According to Lawrie (1988, 1992), olivine and clino- or orthopyroxene were important fractionated phases during crystallization of suite 3 and, compared with other amphibolites in the Virtasalmi belt, the parental magma was derived through a relatively low degree of partial melting. Batch melting and open system fractional crystallization are also suggested by variations in Cr/Zr and Ni/Zr ratios and initial Zr contents (Lawrie 1988).

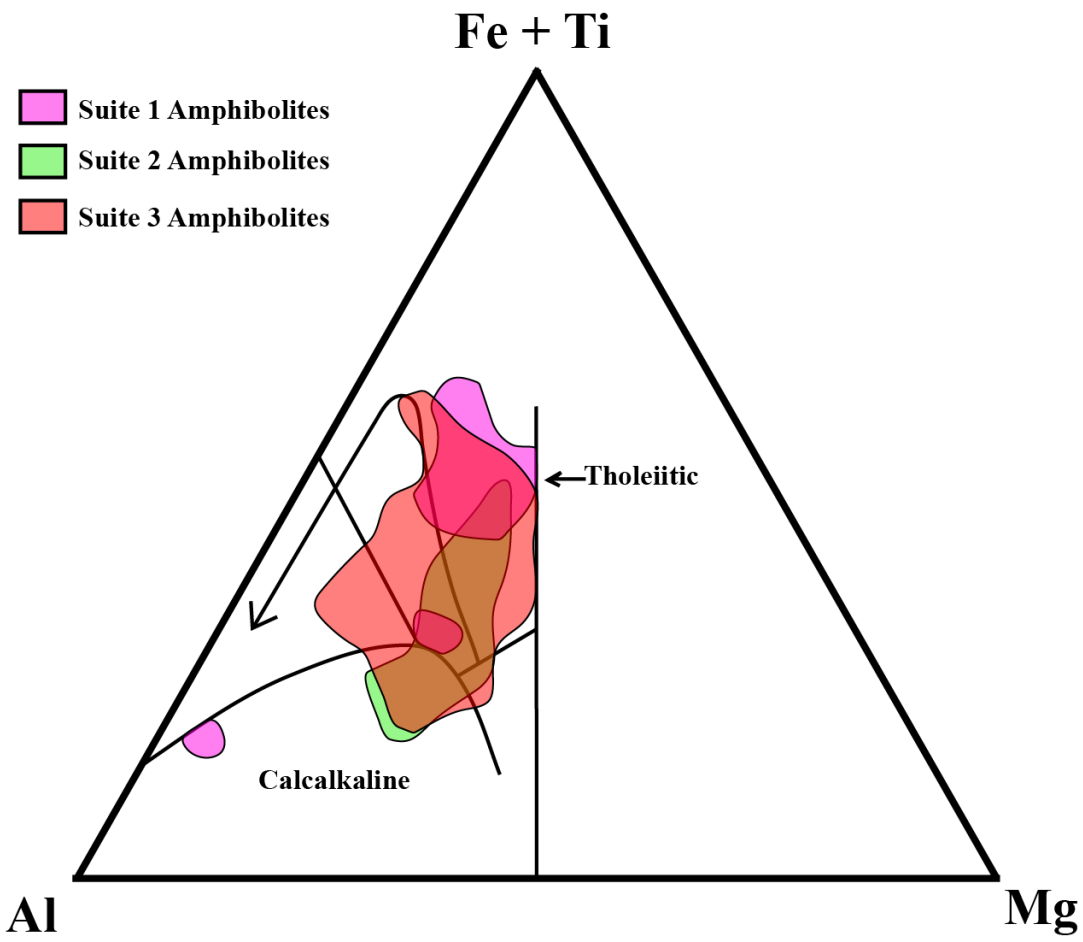

Fig. 4. Jensen cation plot for Virtasalmi amphibolites. Modified after Lawrie (1992).

4.2 Skarn rocks

The term "skarn" is usually connected to lithologies that were formed when a carbonate rock was replaced with silicates. However, in the previous studies of the Virtasalmi area (Hyvärinen 1966; Lawrie 1988), "skarn" has been applied in a broad sense when dealing with metamorphosed sedimentary and volcanogenic rocks where alteration has created Ca-rich silicate mineral assemblages. Lawrie (1992) prefers the term "calc-silicate rock" for the intensively metasomatized rocks in the Virtasalmi belt. Calc-silicate minerals associated with the skarnified rocks of the Virtasalmi area are andradite-grossular garnet, diopside-hedenbergite pyroxene and scapolite mixed with a lower metamorphic assemblage consisting of hornblende, actinolite, epidote and quartz (Lawrie 1992). Lawrie (1988) described 8 types of skarns and their relation to the other country rocks in the Virtasalmi area. Type 1 skarns occur within carbonate layers as sharp bands of calc-silicate minerals. Type 2 skarns are found as concentrations of calc-

silicate minerals embedded in amphibolites in the contact zones between altered amphibolites and carbonate units. Type 3 and 4 skarns occur as ovoid batches of calc-silicates in pillow lavas and lava tubes. Type 5 skarnification is observed in the amphibolite units where carbonate interlayers are generally absent. Type 6 and 7 skarns occur mixed with amphibolite fragments with abundant epidote and magnetite. Type 8 skarns have garnet and pyroxene mixed with abundant magnetite and occur sometimes interlayered with Cu-mineralized amphibolites. Type 5 skarns are chiefly connected to the Cu mineralization while most of the other skarn types are barren. A short description of type 5 skarns is give below after Lawrie (1988).

4.2.1 Type 5 skarns

Type 5 skarns exhibit a gradual change between unaltered amphibolites and massive calc-silicate-dominated skarn rocks. This transition is observed in a scale from 2 cm to 10 m. Mineralogically, the intensity of alteration is indicated by an increasing abundance of andradite garnet. The mode of occurrence of garnet changes from scarce to strong dissemination and where the skarnification is most intense, 90% of the rock can consist of garnet. Diopside and plagioclase exhibit a compositional change in transition zones. Diopside changes to hedenbergite and plagioclase incorporates additional Ca. The intensity of skarn alteration can generally be seen in the increase of bulk CaO in the altered rocks (Hokka and Virnes 2017, Lawrie 1988). Where retrogression has changed the mineral assemblage, epidote and quartz is common. At the Virtasalmi mine, there are places where type 5 skarnified amphibolite units are cut by relatively unaltered amphibolites with disseminated Cu mineralization. These type 5 skarns are interpreted by Lawrie (1988) as a stock work zone for the associated mineralized amphibolites.

5. Geology of the Virtasalmi mine

The Virtasalmi mine, which is now exhausted from resources, is located ~10 km to the south from the Virtasalmi town. Lithological features of the supracrustal rocks around the mine area strike roughly SE-NW and have a steep dip of ~75° towards NE. Intrusive rocks cut other rock units at a high angle. The amphibolite sequence and carbonate unit of the mine area are surrounded by diorite and gabbro intrusions (Fig. 5). The amphibolites are made of a fine-grained, tuffaceous and mineralogically diverse group of rocks, which are commonly sandwiched with each other. The prevailing supracrustal

metavolcanites are cut by various coarser-grained intrusive dikes and sills, which mainly are dioritic and gabbroic in composition. Granitic intrusions are present, comprising coarser-grained pegmatitic rocks and fine-grained aplitic veins, both which are common but not voluminous.

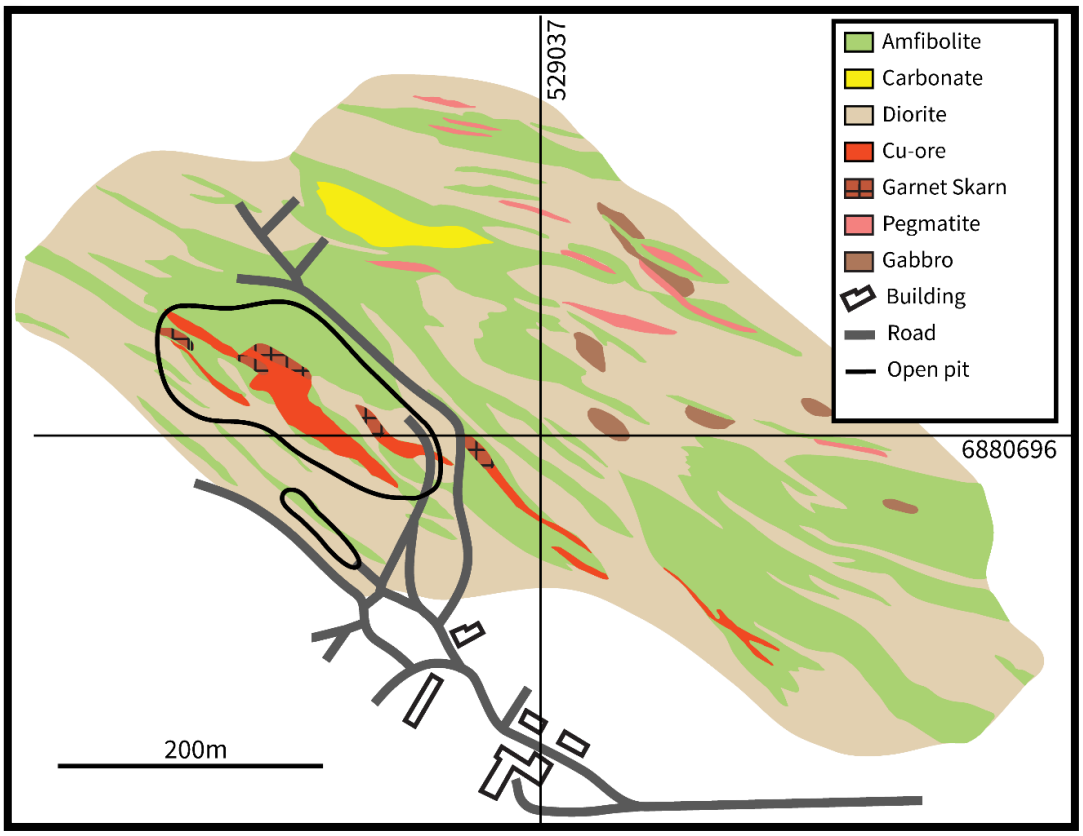

Fig. 5. Lithological map around the open pit of the Virtasalmi mine. Modified after Pekkarinen (2002).

5.1 Amphibolites

There are multiple variants of fine-grained amphibolites in the mine area. They form interlayered mixed rock types where one type dominates while the other(s) forms thin layers or bands (Hyvärinen 1966). Geochemically, the amphibolites of the mine area belong to suite 3 and in some cases to suite 1 (Lawrie 1992). Generally, the amphibolites are made of varying amounts of hornblende, plagioclase and biotite. Hyvärinen (1966) described 3 different variants of amphibolites from the Virtasalmi mine: hornblende-, diopside- and biotite amphibolites.

Hornblende amphibolites are formed of fine-grained, green hornblende and plagioclase with minor biotite. Hornblende amphibolites can be severely fractured and commonly form a mixture with intrusive rocks. Diopside amphibolites consist of diopside-hedenbergite, plagioclase and hornblende with lesser amounts of epidote and garnet (Fig. 6). They are consists of alternating hornblende-poor, pale bands and hornblende-rich, dark bands. Diopside amphibolites are often interlayered with garnet skarns and there is an observable increase of epidote and garnet near the skarn layers. Biotite amphibolites are fine grained, consist of hornblende, biotite and plagioclase and are observed to crosscut diopside amphibolites and their compositional banding (Fig. 7).

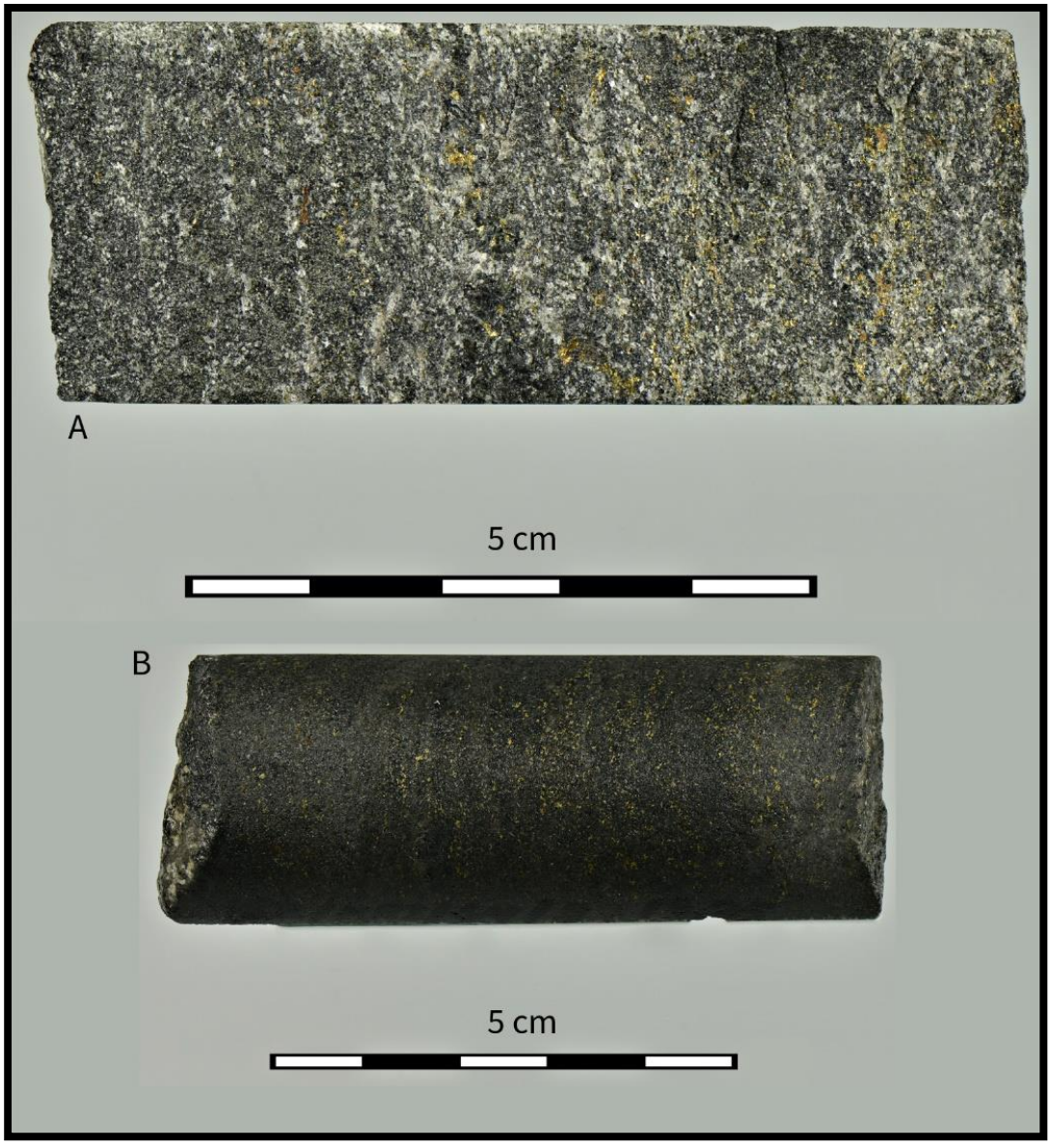

Fig. 6. Diopside amphibolite with disseminated chalcopyrite. A) Split core sample. B) Full core sample, wet. Hole R3, depth 19.75 m. Photos: Geological Survey of Finland 2017.

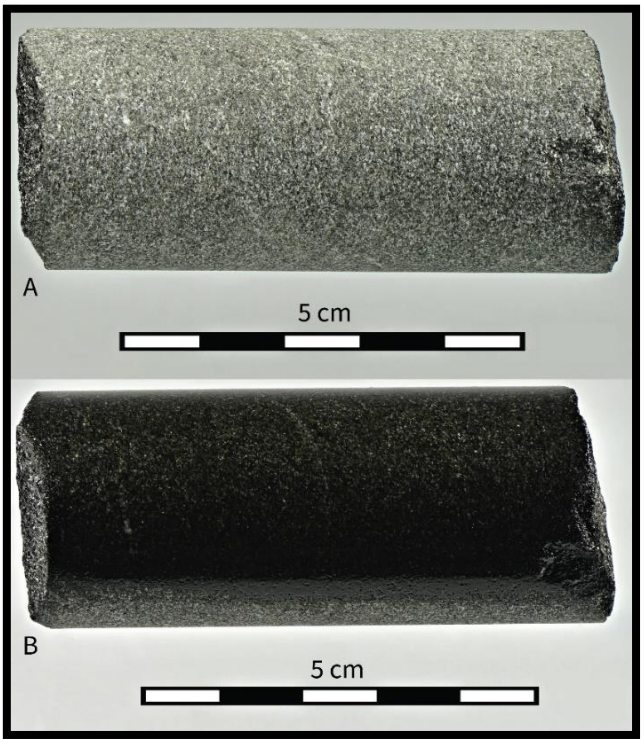

Fig. 7. Non-mineralized biotite amphibolite. A) Dry sample. B) Wet sample. Hole R28, depth 213.70 m. Photos: Geological Survey of Finland 2017.

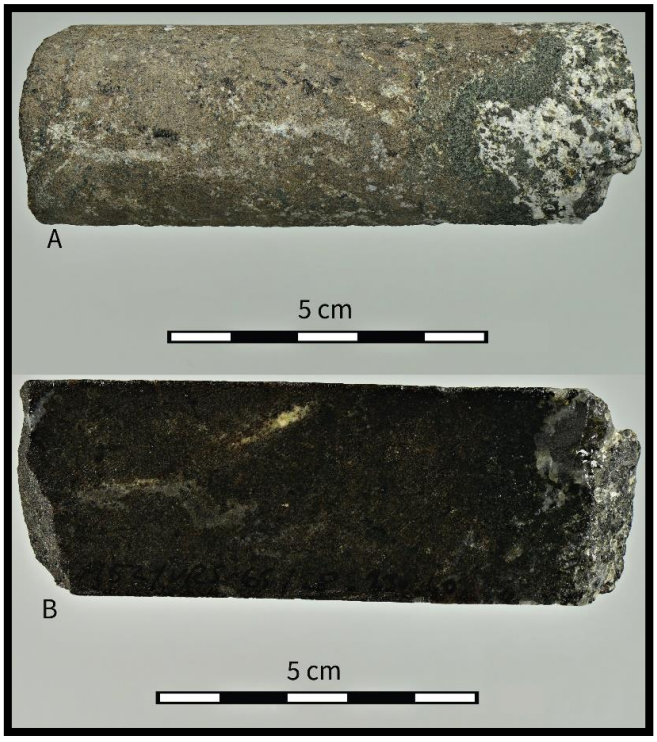

Fig. 8. Weakly mineralized garnet skarn with hedenbergite (green) on contact with diorite. A) Full core sample, dry. B) Split core sample, wet. Hole R28, depth 230.60 m. Photos: Geological Survey of Finland.

5.2 Garnet skarns

Skarnified rock units at the Virtasalmi mine can be 0.5 to 10 m thick and hundreds of meters long and they occur mixed and interlayered with amphibolites. The skarns consist mainly of garnet, which is a solid solution between andradite and grossular or almandine. Also present is hedenbergitic pyroxene, which sometimes is more abundant than garnet (Fig. 8). Epidote, plagioclase and scapolite are common accessory phases while microcline, quartz and sometimes chalcopyrite occur as secondary fracture fillings (Hyvärinen 1966). The calc-silicates in these skarn units occur as fine dissemination, as batches of small minerals or as massive monomineralic zones (Lawrie 1988, Hyvärinen 1966).

5.3 Intrusive rocks

Intrusive rocks represent the prevailing rock types in and around the Virtasalmi mine area. They have various modes of occurrence ranging from large intrusions to dikes, sills and thin veins. They are usually medium grained and gabbroic or dioritic in composition.

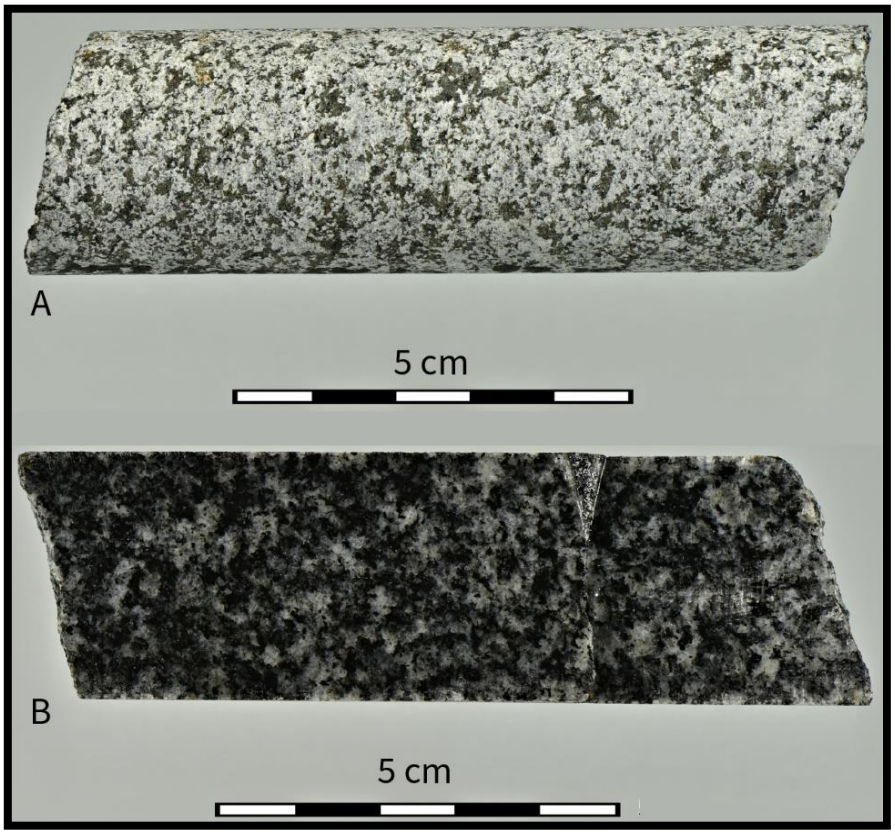

Fig. 9. Diorite. Hole R3, depth 97.15 m. Photos: Geological Survey of Finland 2017.

Granitic intrusive rocks are abundant but do not form large bodies. Especially aplitic and pegmatitic veins are common in fault, shear and fracture zones.

Diorites are the most common intrusive rock type. It is mainly composed of hornblende and plagioclase with minor biotite and cummingtonite (Fig. 9). Less commonly they grade to finer-grained quartz diorites with more biotite and additional quartz (Hyvärinen 1966). Diorites and quartz diorites form a suite comprising rocks of multiple age generations, ranging from early kinematic to late kinematic (Lawrie 1988). Larger gabbro intrusions are common in the Virtasalmi district but at the mine site, they form relatively thin, 4- to 10-meter-wide dikes which cut amphibolites in a high angle. Gabbros consist mainly of hornblende and plagioclase (Fig. 10). In gabbro intrusions amphibolite fragments are common and partial assimilation of the fragments has often happened (Hyvärinen 1966). In terms of timing, the gabbro dikes are mostly early to mid-kinematic (Lawrie 1988).

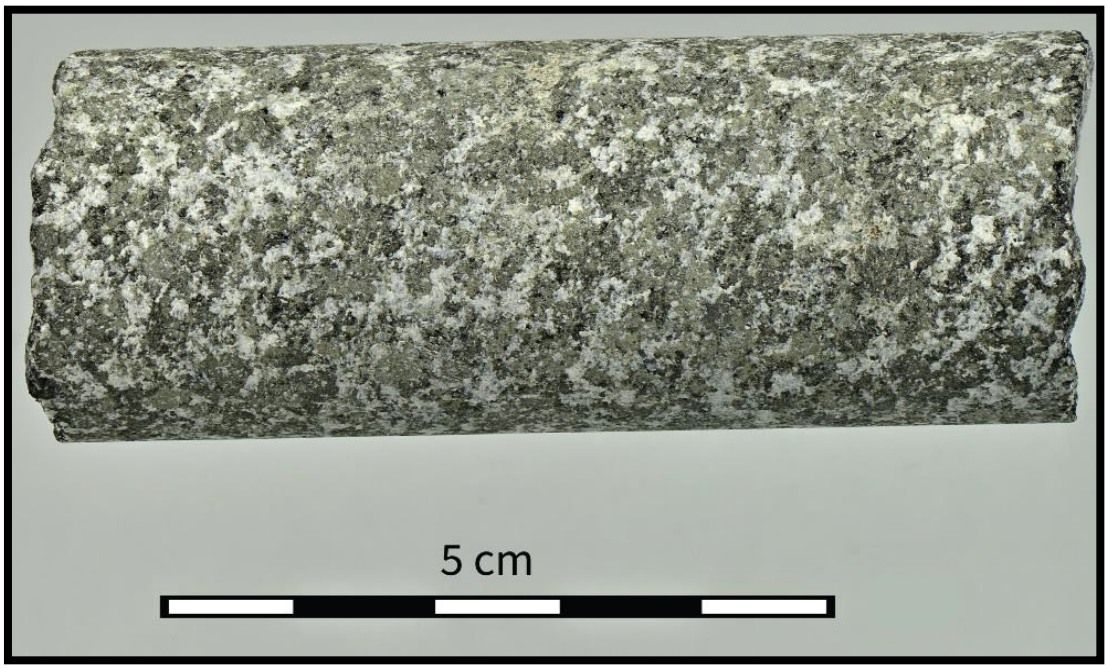

Fig. 10. Gabbro. Hole R28, depth 241.50. Photo: Geological Survey of Finland 2017.

5.4 Local deformational structures

Structurally, the mine area is dominated by a large and tight anticlinal F2 fold, which along with minor structures was described by Lawrie (1988). The F2 fold structure has an axial trend that crosses through the main open pit in a NW-SE direction. The fold has a variable, gentle plunge of ~20° towards north and an inclined axial plane dipping 60° to E. Minor D3 structures are very common around the mine. These F3 folds are upright, have axes plunging 50-70° to SE and have axial planes which dip 60-80° to E. Minor F5 and F6 folds are recorded from the mine area. They commonly refold F3 folds but do not form large structural features. Faulting is common and in places, a major (up to 50 m) displacement has taken place, but the overall effect of faulting on the deposit geometry is poorly confined.

5.5 Copper mineralization

The mineralized zone at the Virtasalmi mine has a strike length of ~650 m long. Under the open pit, the zone continues ~350 m below the surface (218 m below sea level, Fig. 17). The mineralization is irregular and often truncated by barren granitic intrusions. Continuous parts of the mineralization form several lenticular bodies with a general strike and dip of 120/~75°. In surface exposures, the thickness of the mineralized zone

varies from 2 to 30 m, while at depth, the zone becomes narrower and is generally between 5 and 15 m in thickness. Spatially, the mineralization occurs near the contact to the dioritic intrusions (Fig. 5). The major sulfide phases which make up the mineralization are chalcopyrite, cubanite and pyrrhotite. Two modes of mineralization are present: 1) the disseminated type, which is more abundant and common in diopside-rich amphibolite layers; 2) the network type, which is normally associated with garnet skarn layers and their immediate surroundings, but also, less commonly, occurs with fractured amphibolites.

5.5.1 Disseminated Cu mineralization

The grade of the disseminated mineralization varies from low to medium (0.2-0.7 wt.% Cu). Sulfides are either uniformly distributed within the host amphibolite or it form bands in diopside-rich amphibolite layers (Fig. 6). Where sulfide bands occur, they are separated from each other by non-mineralized hornblende amphibolite (Hyvärinen 1966). The disseminated sulfide mineralization is fine grained and chalcopyrite occupies ~80 vol.% of the sulfide minerals (Hyvärinen 1966). Minor cubanite occurs as exsolutions in chalcopyrite. The amount of cubanite exsolutions is higher where the grain size of the dissemination is larger. Only ~6 vol.% of the disseminated ore minerals is pyrrhotite but its proportion increases where dissemination is very weak (Hyvärinen 1966).

5.5.2 Network Cu mineralization

In the high-grade (0.7-8 wt.% Cu) network mineralization sulfides commonly form networks around skarn and amphibolite fragments, but in some places, massive, 5- to 10-cm-long and several-cm-wide lenses of massive sulfide ore exist (Fig. 11). The sulfides in the network mineralization have migrated into structurally weakened skarns and amphibolites during remobilization related to deformation. The major ore minerals which occur in the zones of network mineralization are chalcopyrite, cubanite, pyrrhotite and minor pyrite. Cubanite can make up to 40 vol.% of bulk sulfides while pyrrhotite and pyrite make up to ~15% and chalcopyrite the rest (Hyvärinen 1966). The average grain size of chalcopyrite and cubanite is much coarser than in disseminated ore, reaching 4 cm. On a microscopic scale, bornite, machinawiite, pentlandite, bravoite, sphalerite, molybdenite, linneite, gersdorfite, ludwigite and millerite have been observed as exsolutions in chalcopyrite and pyrrhotite (Hyvärinen 1966).

Fig. 11. Network mineralization in diopside amphibolite. A) Full core sample, wet. B) Split core sample, dry. Hole R28, depth 220.20 m. Photos by Geological Survey of Finland.

5.6 Remobilization of the sulfides

Minor mobilization of sulfides has taken place during deformation phases D1 and D2. This is mostly expressed as elongated sulfide mineral growth in the S1 and S2 direction (Lawrie 1988). Major remobilization, recrystallization and upgrading of the Cu grade have occurred during D3 as sulfides adjusted towards low strain zones. In minor F3 hinge zones, recrystallization has created lenticular massive chalcopyrite pods and network mineralization. Similar features can be seen on the limbs of F3 folds where sulfides form elongated pods and chalcopyrite occurs as fracture filling (Lawrie 1988).

5.7 Local stratigraphy

An interpretation of the local stratigraphy of the Virtasalmi mine was presented by Lawrie (1988) based on field evidence from underground mapping, especially in the

production areas under the open pit at levels 55, 140 and 335 meters below the surface. An inferred and simplified stratigraphical column after Lawrie (1988) is illustrated in Fig. 12.

The lowest stratigraphic unit, A, consists of relatively homogenous amphibolite with strongly skarnified zones near the contact with the overlying unit B. The unit A skarn zones are discordant with respect to the unit B banding and the sharp contact between A and B. Unit A is generally barren, but some chalcopyrite dissemination is present near the A-B contact. Unit B comprises hedenbergite-rich, banded amphibolites and skarn layers, with the thickness of the banding and layering varying greatly from some centimeters to some meters. Banding and layering are subparallel to the A-B contact. Unit B is the main ore horizon as it contains a strong sulfide dissemination in its basal part in addition to lenses of network mineralization. Unit C consists of interlayered hornblende and diopside amphibolite and is generally free of sulfide mineralization. The contact between units B and C is unconformable and crosscuts the banding and layering of unit B and was used as a way-up indicator by Lawrie (1988). The two uppermost stratigraphic units, D and E, are made of thinly banded amphibolites overlying conformably unit C. Unit D is free of sulfide mineralization but does have some skarnified networks, above which unit E contains weak sulfide mineralization in the form of disseminated pyrrhotite.

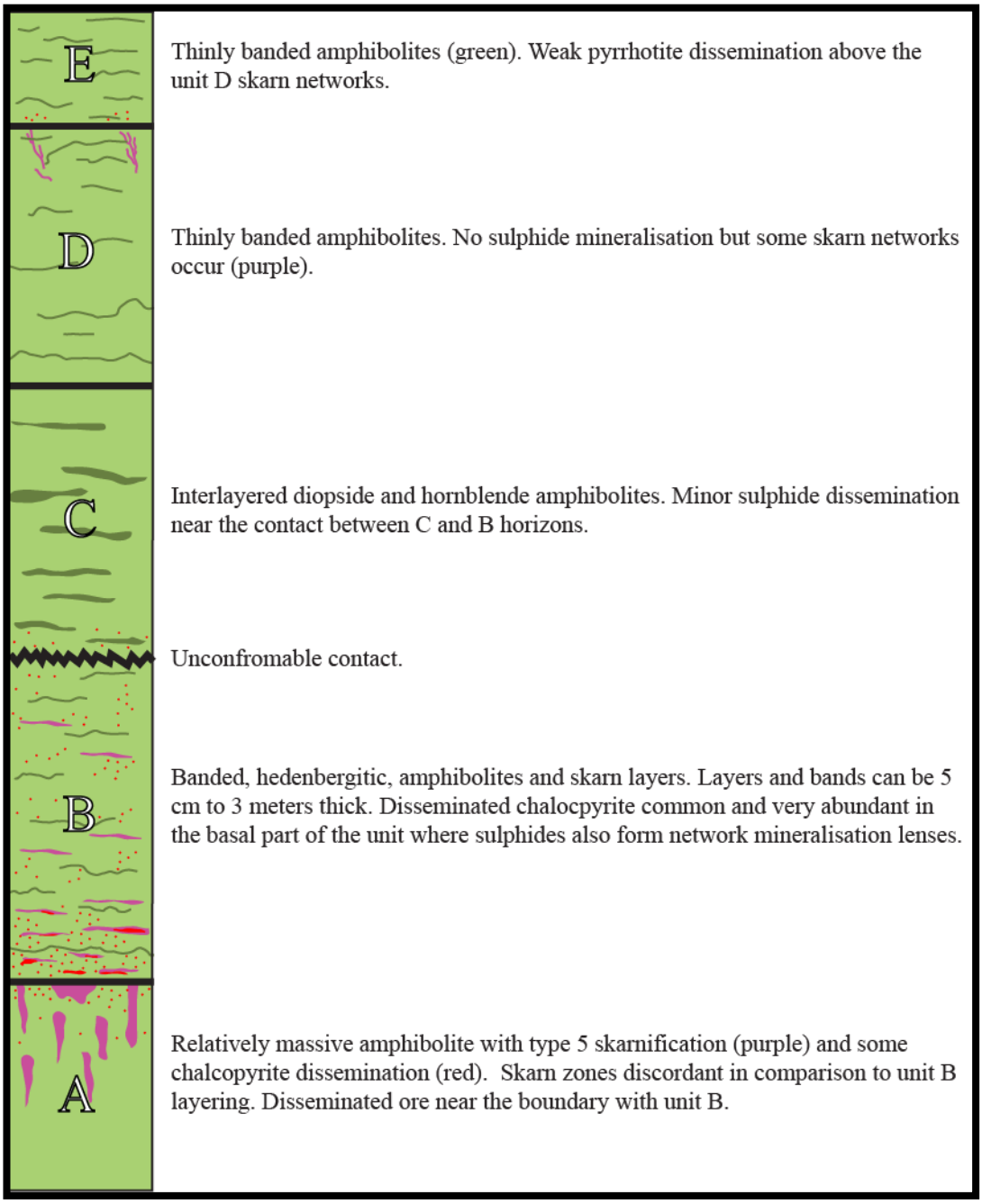

Fig. 12. Simplified and inferred local stratigraphy in the Virtasalmi mine area after Lawrie (1988).

5.8 Relative timing and genesis of the Virtasalmi mineralization

During the operation of the Virtasalmi mine, Hyvärinen (1969) suggested that the mineralization was of a contact-pneumatolytic type and that it was likely to be late-orogenic and connected to the emplacement of the diorite-quartz diorite intrusive suite. However, Lawrie (1988) showed that the Virtasalmi area has a very complex tectonic history, which is accompanied by several sets of intrusions with different ages and these

intrusions, especially the diorites, postdate the amphibolites. The majority of the intrusions do not show early S1 and S2 metamorphic fabrics, which are observed in the amphibolites and to a lesser extent in the sulfides. Lawrie (1988) suggests that the mineralization is of a volcanogenic exhalative type as evidenced by the locally outcropping pillow lavas and lava tubes and the overall N-MORB affinity of the amphibolites, which imply an oceanic and possible passive continental margin setting. In addition, the basal unit A contains skarn stockworks formed at a high angle to S0, and such features as banding of the amphibolites. Above these skarn stockworks, the most abundant mineralization appears in basal parts of unit B where skarn layers are subparallel to S0. There are also amphibolite suites where leaching has taken place and suites where mobile elements, such as Ca and Cu, have elevated concentrations. Suite 1 amphibolites with low CaO and elevated Na_2O and Si_2O represent the rocks from which leaching has extracted metals. The suite 3 amphibolites, common within the mine, display elevated CaO values with high S and Cu and in turn represent rocks where metasomatic fluids has caused alteration and precipitation of sulfides near or at the sea floor (Lawrie 1988).

6. Methods and materials

6.1 Copper grade modeling

The data utilized in this thesis have been collected and created by the Geological Survey of Finland (GTK) and Outokumpu Oy (OKU) during the exploration and operation of the Virtasalmi mine, between 1964 and 1982. The historical data have since been recovered from the national archive for the use in this thesis. The original data consist of hand- and machine-typed core logs, hand-drawn technical mine plans and geological profiles and maps. At least six geologists were responsible for the collection of the original core log data during the exploration and operation of the mine. The core logs were digitized by hand using Excel and converted to a geological database, which includes collar, survey and assay files. The majority of the maps were georeferenced and most relevant ones were redrawn in a digital form. These maps were used for quality checking of the geological database and the mine plans were used to reconstruct the original mine infrastructure. The assay file contains Cu analyses from a total of 239 drill holes, totaling 2995 individual analyses and ~4760 m meters of analyzed drill hole

core with an average sample length of 1.6 m (Tables 1, 2 and 3). Only copper and sulfur values have been consistently reported in the original drill logs. Gold, silver and iron contents have been only occasionally recorded and no whole-rock geochemical data have been recorded. The drilling machinery has varied during the drilling years and the drill core diameter has either been 21 or 32 mm. Original logs or technical reports which are available are unspecific about which core diameter was used and for which collars. Likewise, no reference to the method of Cu analysis was found in the Virtasalmi mine

technical reports.

Table 1. Total collar summary.

Total drill holes	239
Total drill hole length	30582.13 m
Total samples collected	2995
Total sample length	4764.63 m
Average sample length	1.59 m
Average Cu grade	0.633 wt.%

Table 2. GTK collar summary.

Drill holes (surface)	83
Drill hole length	16475.51 m
Sample count	880
Total sample length	1947 m
Average sample length	2.21 m
Average Cu grade	0.707 wt.%
Operation years	1964-1966

Table 3. Outokumpu Oy collar summary.

Drill holes (underground)	156
Drill hole length	14106.62 m
Sample count	2115
Total sample length	2817.63 m
Average sample length	1.33 m
Average Cu grade	0.602%
Operation years	1973-1982

The original drill core logs were placed in a local coordinate grid, which was part of a custom regional grid created by the GTK for regional exploration and mapping. In order to facilitate the handling of the database with the GEOVIA Surpac 3D modeling software, the local coordinate grid was converted to the EUREFIN coordinate system. This was done using the Arc Map GIS software where collar maps containing surface hole location data were first georeferred based on the remaining infrastructure. The full database was input to ArcMap, mirrored and moved to its correct location by georeferencing based on the surface collar map. The elevation data in collar file was originally measured partly in a local system and partly in the national n43 system. The collars whose elevation was recorded in this local system were converted and the whole database was updated to the national n2000 elevation system. In addition, the surface collars were snapped to a high resolution topographical LIDAR surface (Light Imaging, Detection, And Ranging) provided by the GTK and the underground collars were adjusted accordingly. Visual comparison between the collar file and reconstructed mine infrastructure was used to quality check the elevation data conversion. In the assay file, copper values which were either missing or had a zero value were set to 0.0001.

The cut-off grade of 0.2 wt.% Cu was chosen to display the general extent of the mineralization. The raw data are very skewed towards the low Cu grades with ~38% being 0.19 wt.% or less (Fig. 13). The mineralization was divided into 13 main crosscut profiles and 1-3 supporting profiles between them (Fig. 14). The main crosscut profiles are set according to the original drilling plan. The collar profiles have a 12.5-m distance between each other in the vicinity of the open pit and 25-m dispersion SE of the open pit. The additional crosscut profiles (drill core data) were used as support where

underground stopes were present according to the reconstructed mine infrastructure. The wireframes were not directly snapped to Cu grade values since the collars were not perfectly aligned and this caused trouble in validation. Instead, the wireframes were set visually as close as possible to the Cu grade extents. The mineralized amphibolite is often cut by intrusive veins and thus inner gangue zones had to be included within the wireframes to ensure compatibility while connecting wireframes. The inner gangue was avoided but non-mineralized sections were included where wireframe simplification was necessary and where the gangue was surrounded by mineralized rock.

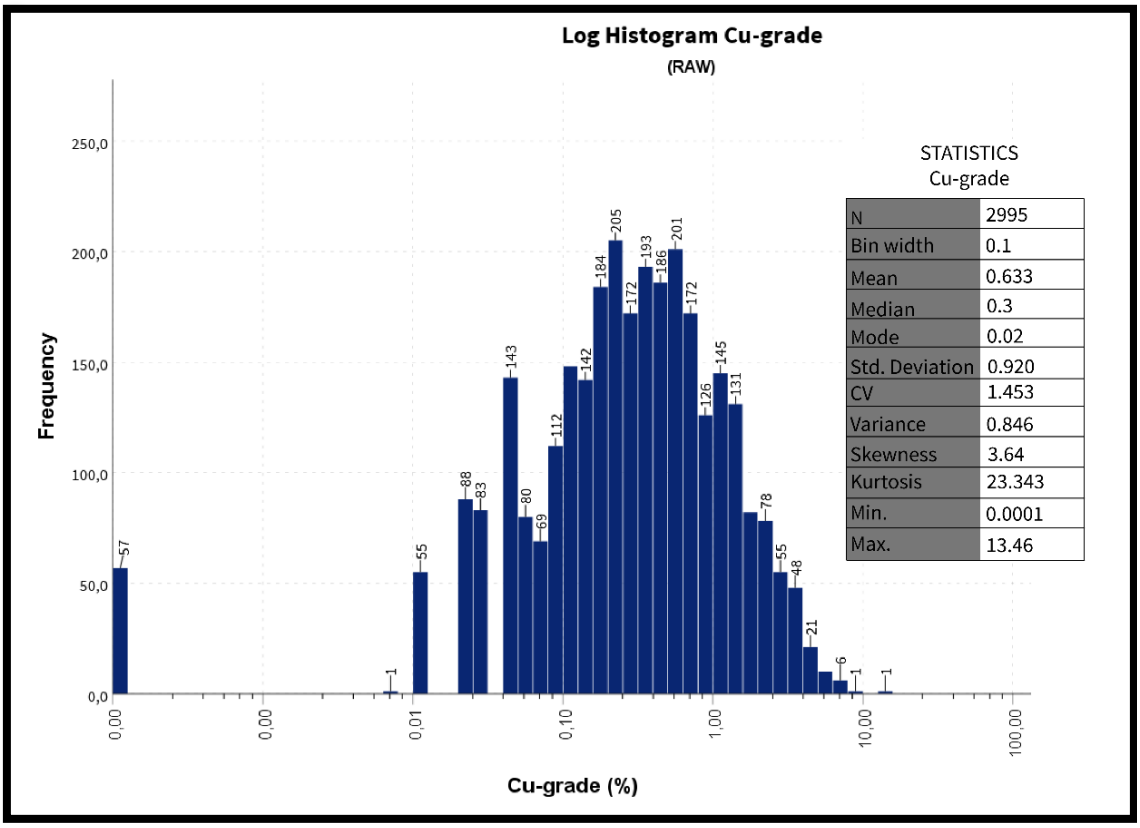

Fig. 13. Cu grade loghistogram and statistics.

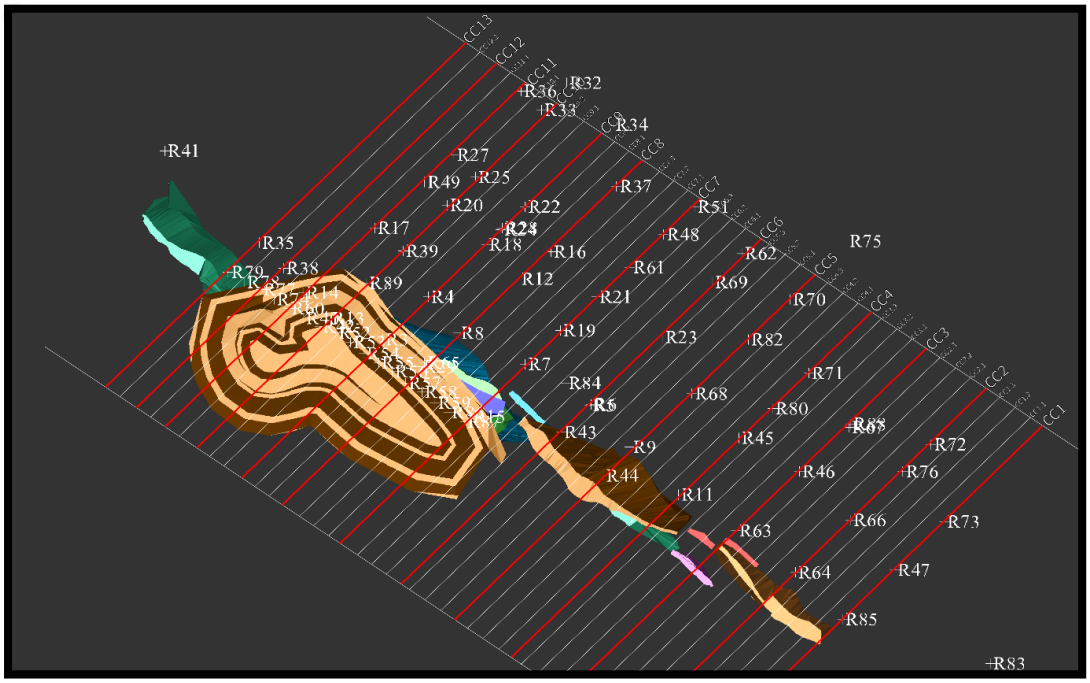

Fig. 14. Crosscut profile plan and the location of the open pit and underground stopes. Primary profiles in red and additional profiles in white.

The Cu mineralization solids were closed by copying and extruding the fringe wireframes to a complete close using half of the distance of the crosscut profile distance ~6 m in this case. The original sampling has been selective and raw sample lengths vary between ~10 cm and ~5 m (Fig. 15). The selective sampling has not caused a considerable "nugget effect" even though there is some correlation between short samples and higher Cu grade (Fig. 16).

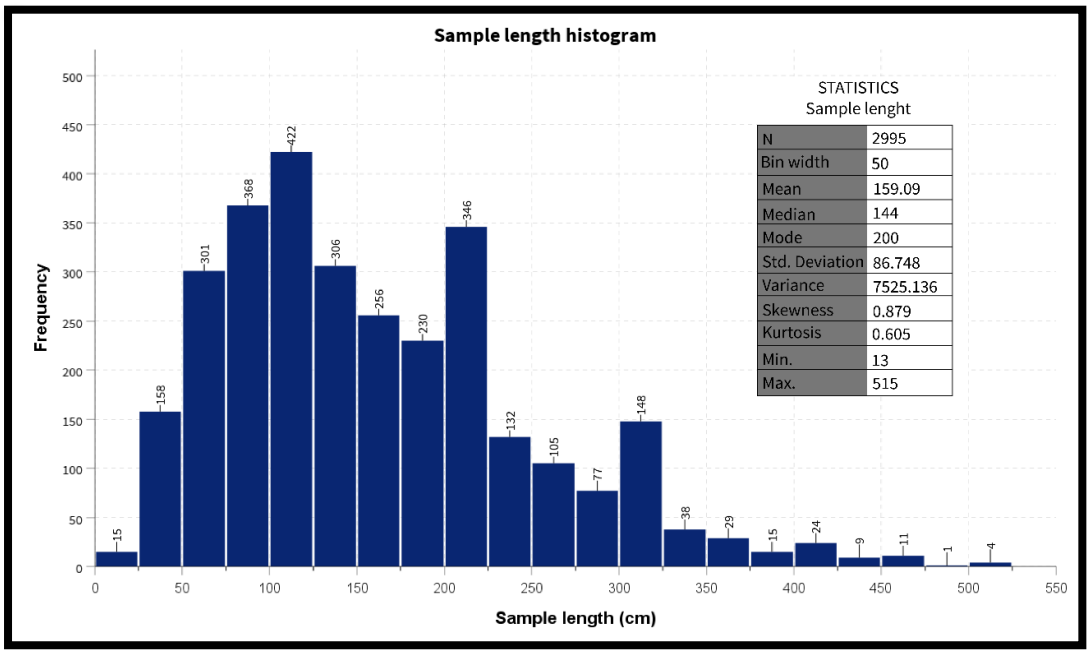

Fig. 15. Sample length distribution of the raw data.

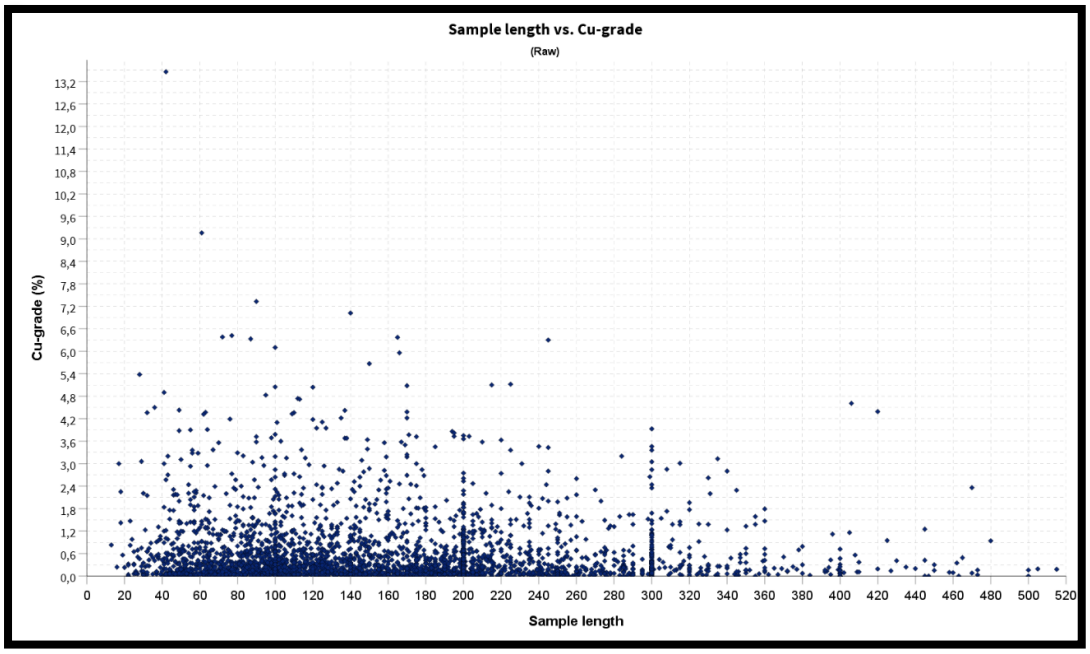

Fig. 16. Correlation between sample length and Cu grade.

6.2 Open pit, stope and mineralization solid tonnage estimation

In order to compare the mineralization model with historical records and quantify the correctness of the model, tonnages were estimated for the open pit, underground stopes and to the whole mineralization solid (Figs. 17 and 18). Significant errors were expected

to occur when calculating the total tonnage because the technical reports obtained for this study did not state the methods used for production estimation at the Virtasalmi mine. The only historical reference from Hyvärinen (1966) is a crude average density of 3.2 g/cm^3, which was used during an early mineralization potential estimation by the GTK.

To make the tonnage estimation more precise, drill core samples were collected from typical mine site lithologies and the samples were analyzed for their physical properties including density (Table 4). The sampled rock types included gabbro, diorite, non-mineralized amphibolite, non-mineralized garnet skarn, amphibolite with disseminated mineralization and network-mineralized garnet skarn. The densities of the above-mentioned rock types were applied together or individually for tonnage and production estimation.

The total excavated rock tonnage from the open pit was calculated by using the average rock density of all drill core samples, since a large amount of waste rock had to be quarried with the ore. For estimation of the excavated rock mass from the underground stopes, an average density of mineralized rock was used to optimize for the lower amount of waste rock (Table 4).

Ore production and mineralization potential tonnages were calculated by applying the disseminated mineralization density for the "low-grade" zone and the network mineralization density for the "high-grade" zone of the mineralization solids (Table 4).

Table 4. Rock densities from drill core samples.

Average rock density	3.226 g/cm^3
Average mineralized rock density	3.5 g/cm^3
Amphibolite (disseminated mineralization)	2.84 g/cm^3
Garnet skarn (network mineralization)	4.175 g/cm^3

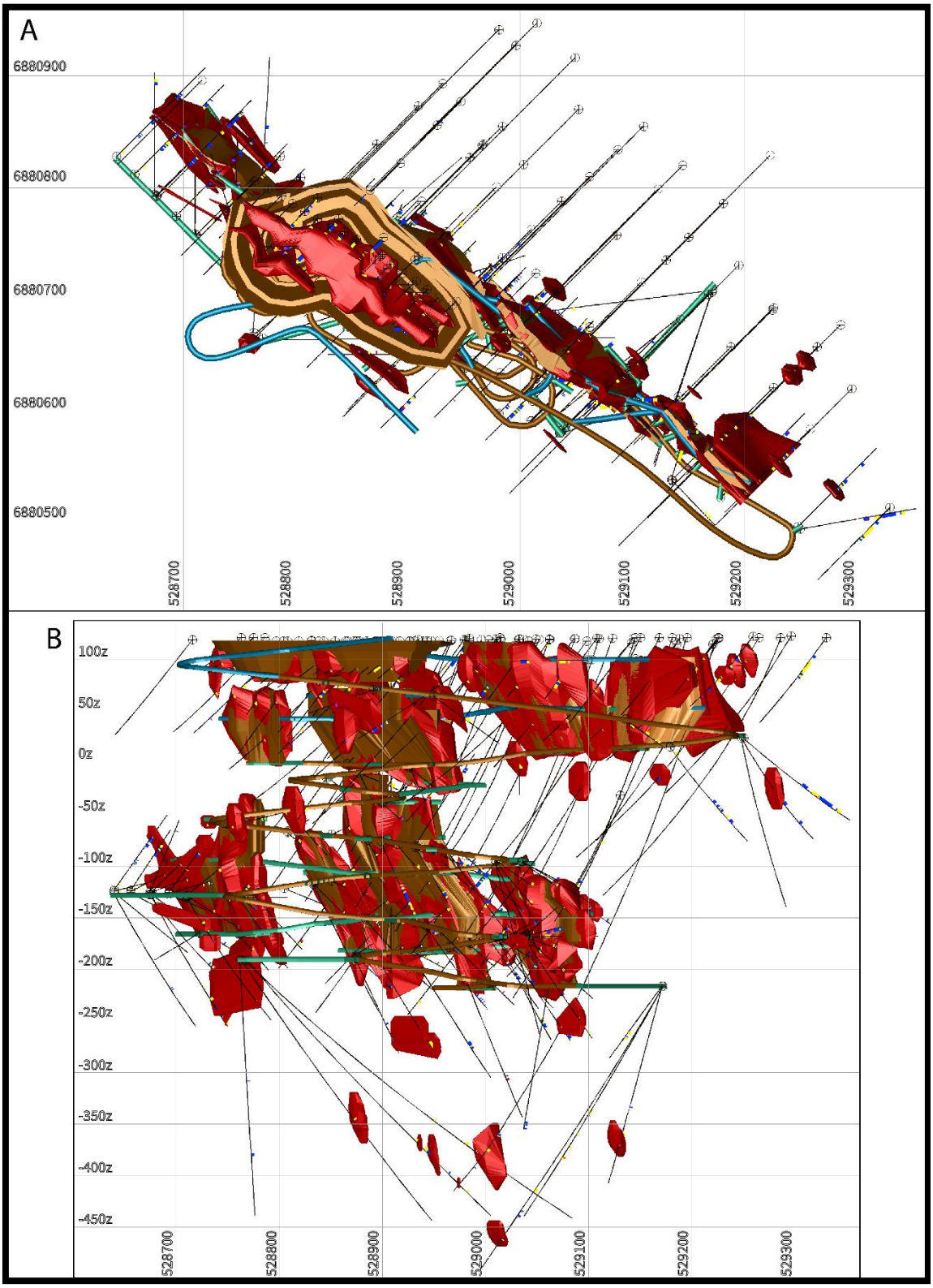

Fig. 17. General extents of the mineralization with cut-off at 0.2 wt.% Cu and the mine infrastructure including the open pit and underground stopes. A) Looking down. B) Looking north.

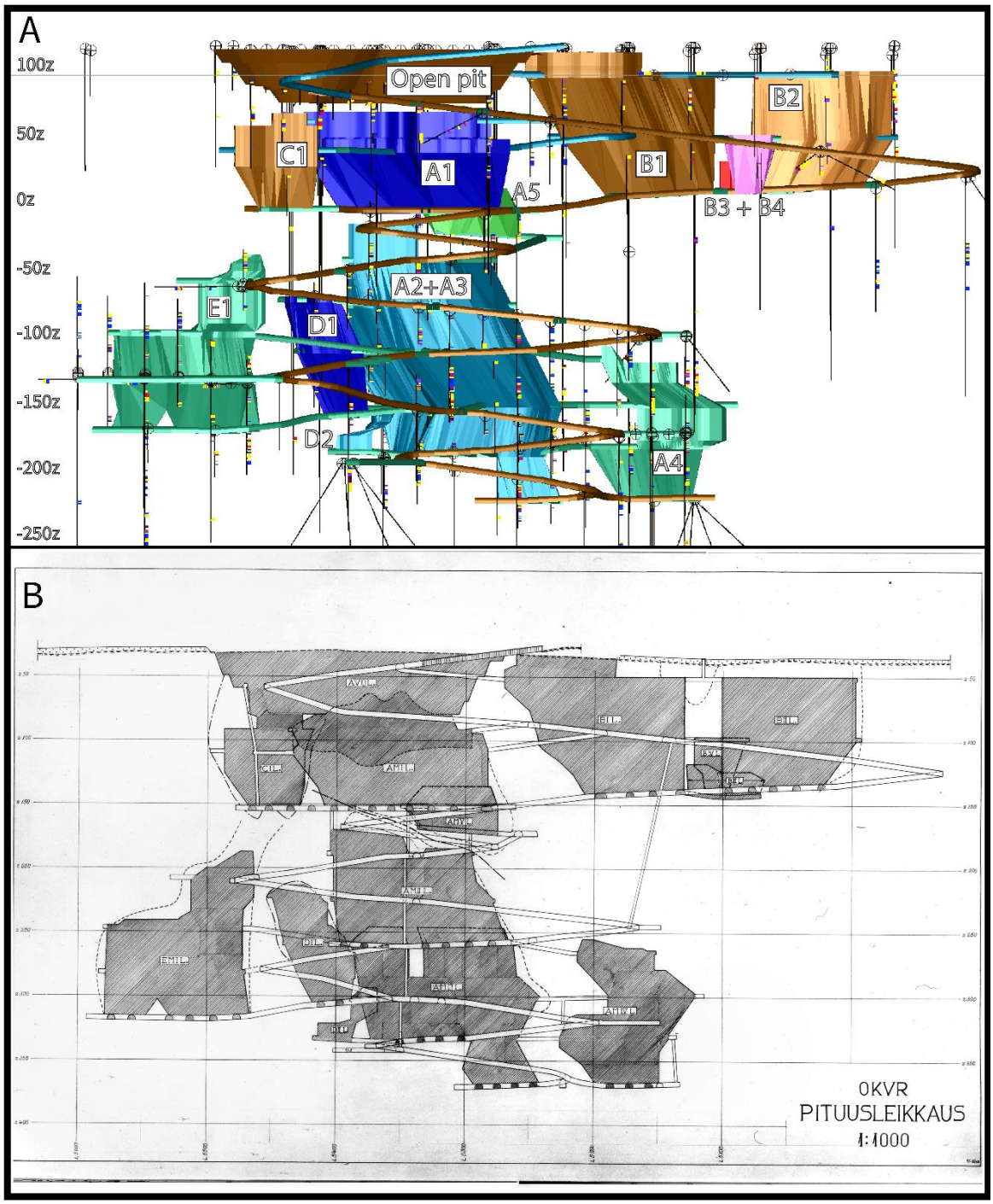

Fig. 18. A) Reconstructed mine infrastructure. Looking NE. B) Original profile from Outokumpu Oy technical reports.

6.3 Coordinate grid and elevation system

During the exploration and operation of the Virtasalmi mine, all drill hole locations were recorded in a local coordinate grid, which was established by the Geological Survey of Finland in 1964. This local coordinate grid was set up at a 45-degree angle so

that in the Virtasalmi area, the coordinates grew towards NW and NE. Setting up a custom coordinate grid is possible in the GEOVIA Surpac and Arcmap 10 softwares, but to make the data set compatible with the GTK database, it was converted to the EUREFIN coordinate system. A mathematical approach was initially attempted but this proved to be a confusing method and ultimately resulted in erroneous coordinate conversion. A far better result was achieved by loading the raw collar location data to Arcmap 10, mirroring the dataset to match the x-y axes of modern maps and moving and rotating the dataset to its correct location and orientation by georeferencing according to original, georeferred collar maps. Twenty collars were moved by hand to their correct locations and an algorithm moved the rest of the collars accordingly. The distance between two collars in a profile changed less than a meter (10–70 cm). Comparison between the fixed collar positions and original, hand drawn, georeferred maps showed a maximum of ±2-meter error.

During the exploration, the Geological Survey of Finland recorded the elevation data (Z coordinate) directly in the old national N43 system. Afterwards, during the operation of the mine, Outokumpu Oy recorded the collar elevations and planned the mine operations in their own local Z coordinate grid. The Z0 of this local grid was placed at the height of 150 (N43). To make the dataset work better with modern softwares, the local Z coordinates were converted, first to the old N43 system and then to the modern national N2000 system, which accommodates for postglacial lift around the area. Furthermore, a high precision LIDAR topographic surface, provided by the GTK, was compared with the corrected collar locations. Most of the original collar positions were situated underneath the LIDAR surface with an average displacement of 1.7 m. Collars were above the topographic surface only around the Hällinmäki hill, which has since been mined flat. The surface collars (R collars) were tied to the LIDAR surface and the underground collars were adjusted accordingly with +1.7 m displacement to unify the elevation dataset. Therefore, the full conversion from local Z coordinate grid to the modern N2000 elevation system with additional correction according to the LIDAR surface and glacial uplift is as follows:

$$Z_{N2000} = (150 - Z_{local\_grid}) + 0.34 + 1.7 \qquad (1)$$

where 150 is the Z0 in the old national N43 system, 0.34 is the correction for glacial uplift and 1.7 is the average correction according to the LIDAR data.

7. Results

7.1 Collar and mineralization distribution and general extents

The diamond drill holes are distributed roughly in two different sets according to the data from collar and survey files. The “R collars” were drilled by the Geological Survey of Finland (GTK) during exploration. They originate from the surface and were drilled roughly towards SW, perpendicular to the general strike of the mineralization. The “HM-collars” were drilled by Outokumpu Oy during the operation of the mine. They originate from underground tunnels and have been usually drilled in a fan shape towards various directions. The selective sampling method implemented by the GTK and Outokumpu Oy is seen in the data from assay files. The sample length ranges from some tens of centimeters to several meters (Figs. 15 and 19).

By connecting wireframes drawn with cut-off grade of 0.2 wt.% copper on multiple crosscut profiles, three main mineralization bodies can be distinguished (Fig. 20). Together they have a total strike length of ~626 m (NW – SE) and the maximum depth of mineralization is ~344 m (mineralization bodies A and C). All three bodies form out of one or more mineralization lenses which dip steeply towards NE (Fig. 21). The mineralization is most abundant near surface at mineralization body A where the mineralization is at its widest (Fig. 20). The body A, and the other mineralization bodies, become progressively thinner at depth. Below 250 m (sea level) the mineralization occurs as small lenses under the body A. These small pods also exist under the mineralization B, but at a shallower depth (Figs. 20 and 21).

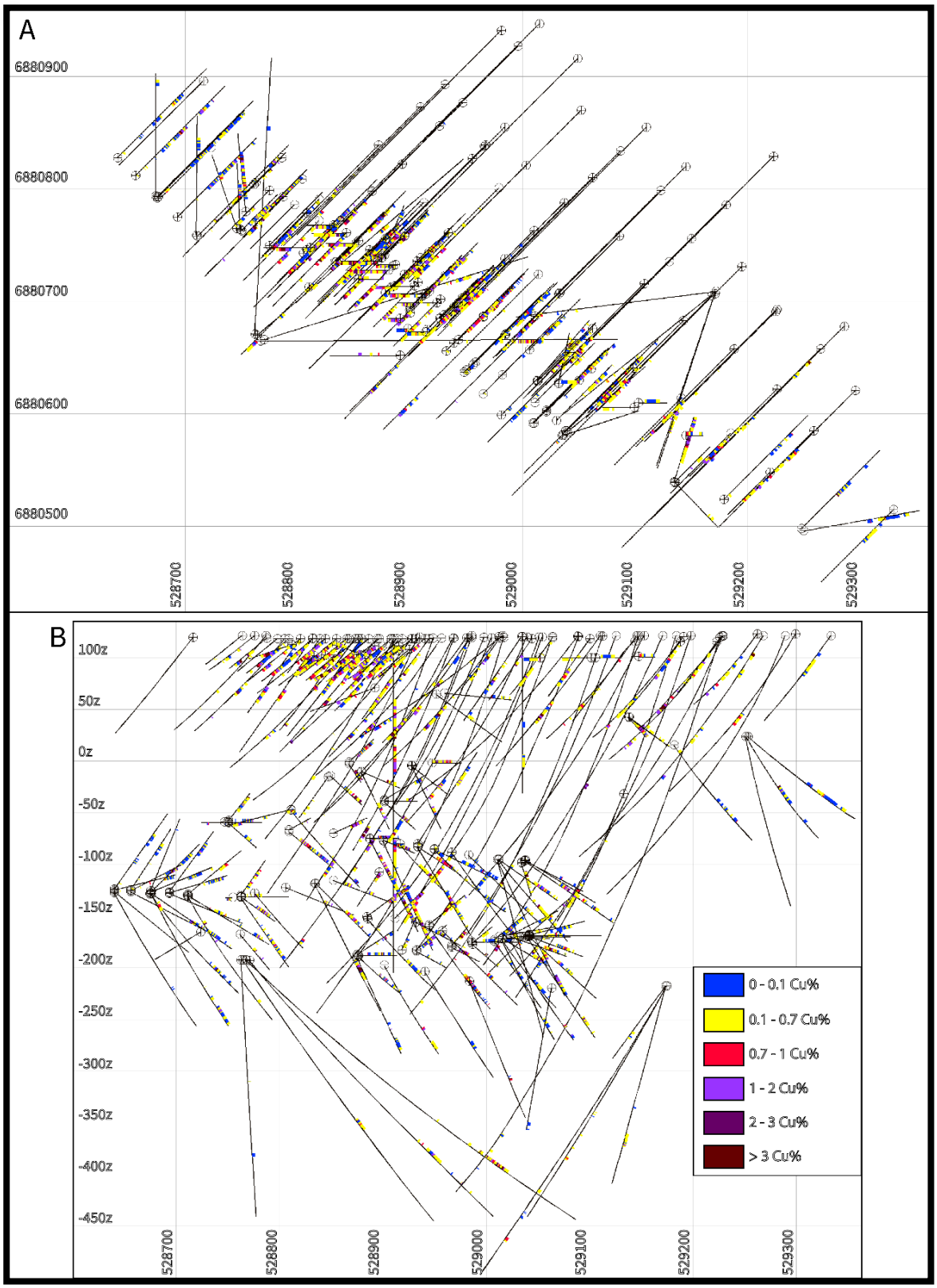

Fig. 19. Collar and Cu grade distribution. A) From above. B) Looking north.

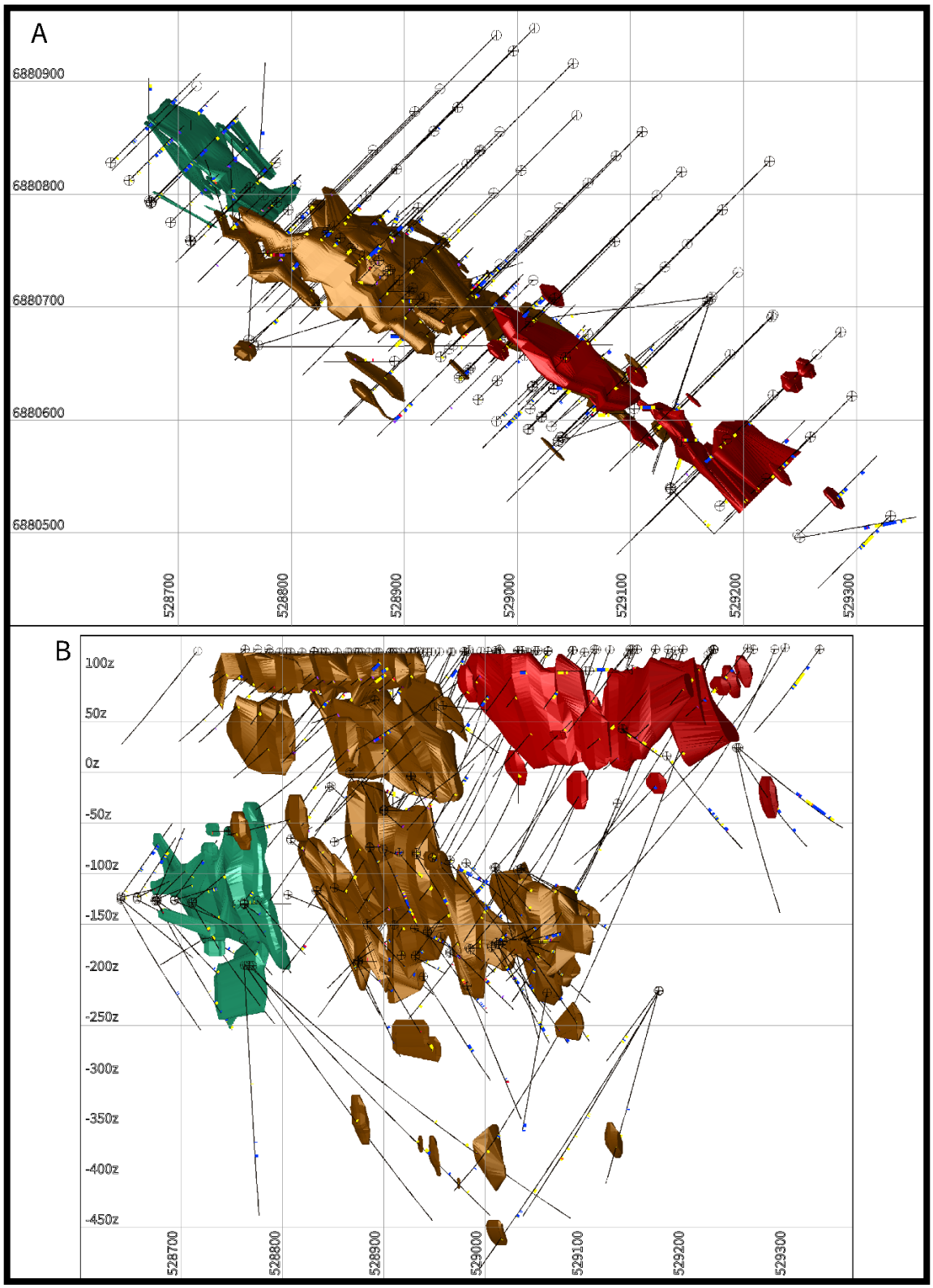

Fig. 20. Distribution of mineralization, cut-off at 0.2 wt.% Cu. A) From above. B) Looking north. Mineralization coloring according to original division: A (brown), B (red) and C (green).

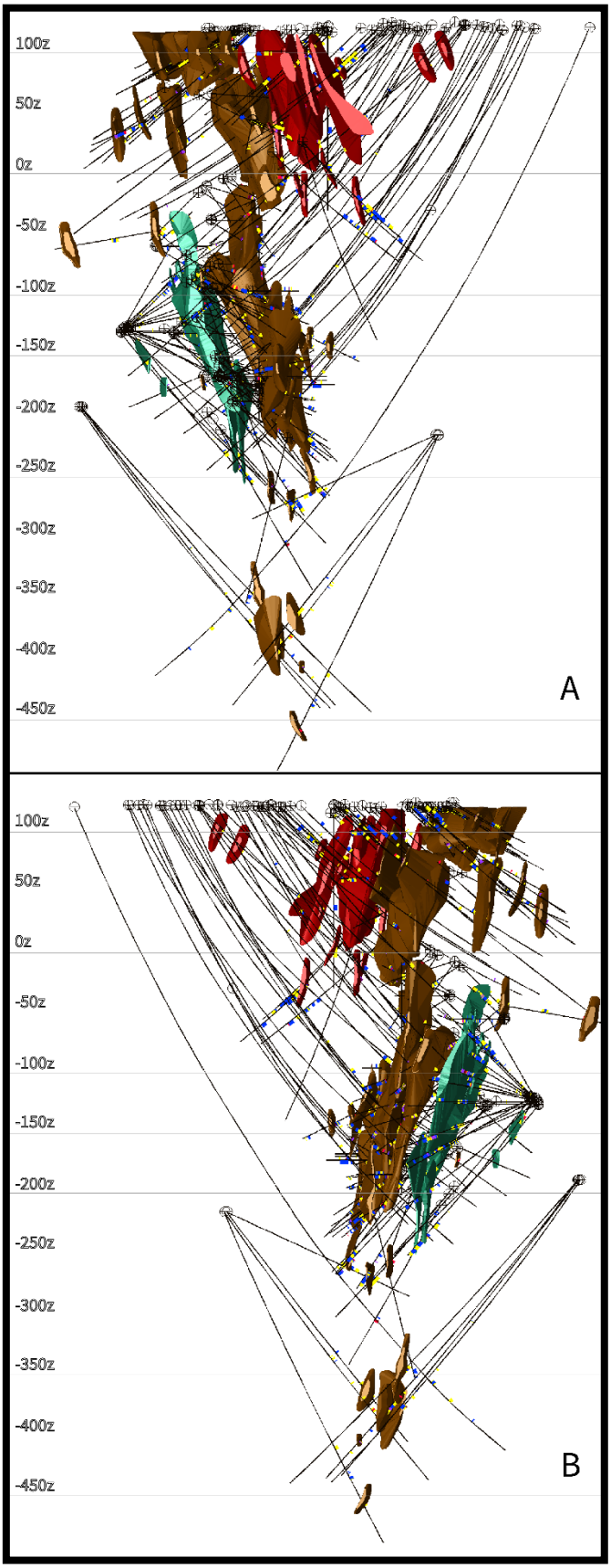

Fig. 21. Distribution of mineralization. A) View towards NW (310°/00. B) View towards SE (130°/00).

7.2 Distribution of high-grade mineralization

High-grade (<0.7 wt.% Cu) zones are distributed in relatively thin lenses and are generally surrounded by disseminated mineralization (Fig. 23). The thickness of the lenses is 1–3 meters but occasionally they can be 7–8 meters thick. The strike length of an individual lens varies greatly, being from less than 10 meters to more than 100 meters at best. High-grade mineralization is most abundant in the mineralization body A (Fig. 20) in the open pit and under it in the A1–A3 underground stopes (Fig. 18), but generally some high-grade sheets are associated with nearly all mineralization lenses. The high-grade zones are usually connected to garnet skarns or occur in their immediate proximity. Some remobilization has taken place and intrusive diorites are occasionally highly mineralized next to garnet skarn units (Fig. 22).

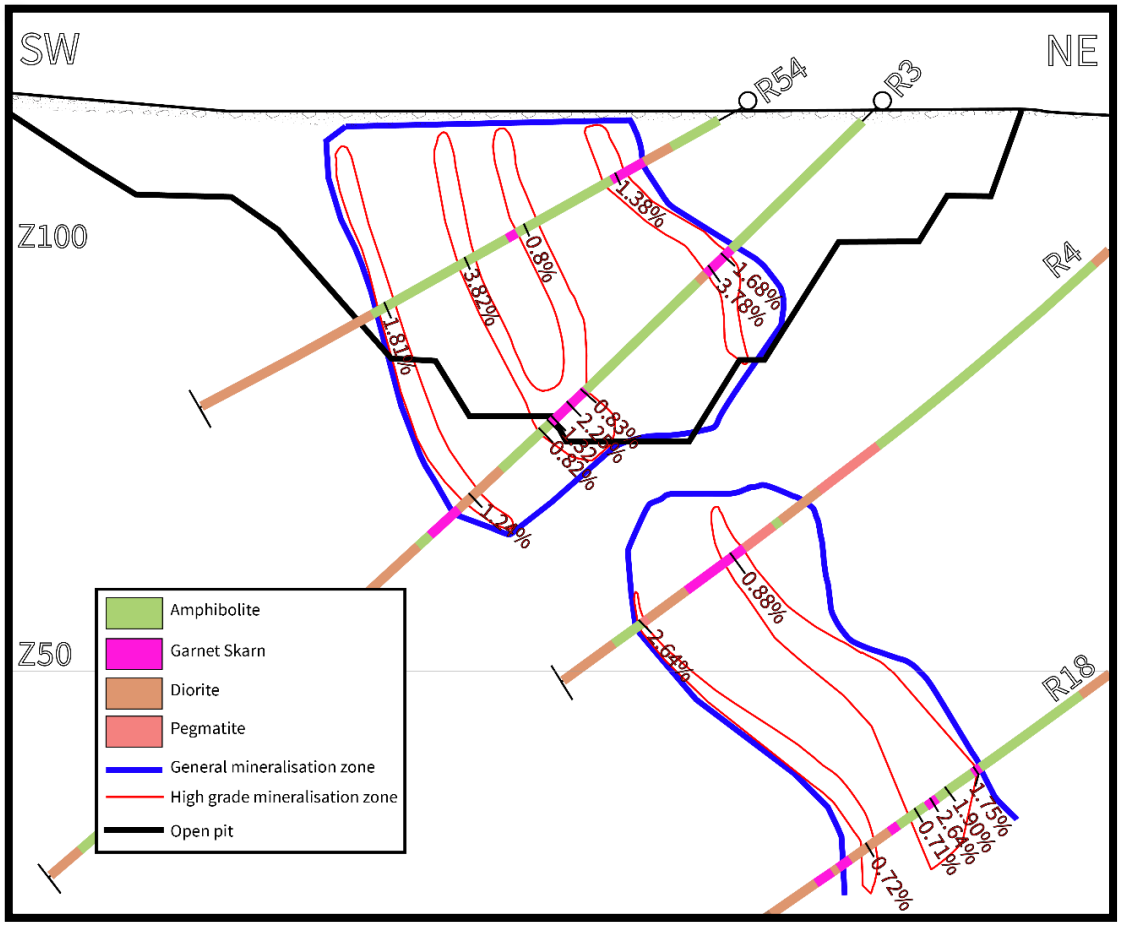

Fig. 22. Crosscut section through the open pit (CC9 in Fig. 12). High copper grades are generally connected to the vicinity of garnet skarns.

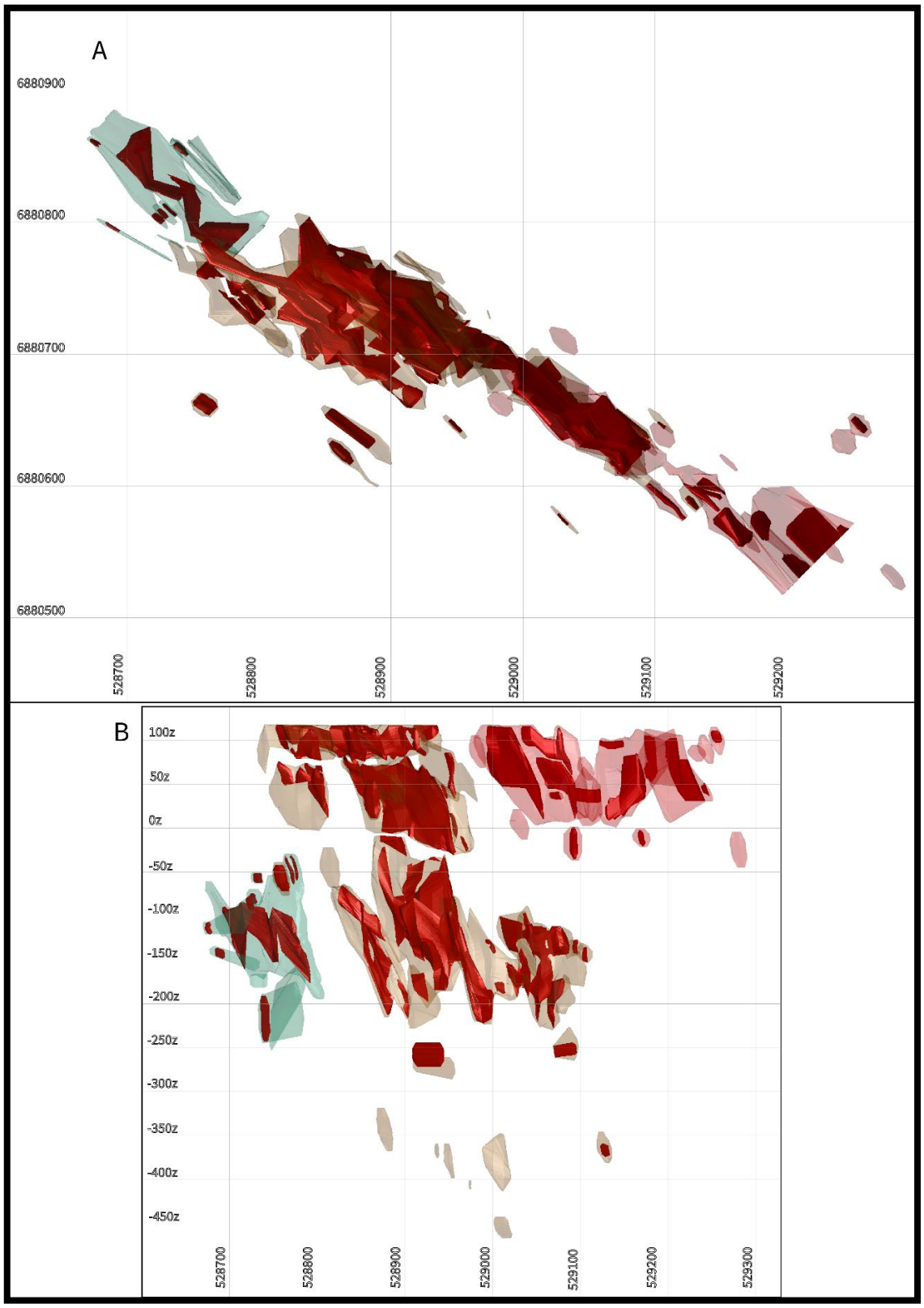

Fig. 23. High-grade (>0.7% Cu) copper mineralization lenses (red) inside general mineralization solids (transparent, 0.2 wt.% Cu cut-off). A) Looking down. B) Looking north.

7.3 Resource estimation

In the present study, a crude pre-mining mineralization estimate, including all mineralization lenses, was calculated for the model using a general cut-off of 0.2 wt.% Cu for low grade mineralization and >0.7 wt.% Cu for high-grade network mineralized zones. Disseminated and network mineralization lenses were calculated with separate densities to increase accuracy (Table 4). The results indicate that the Virtasalmi mine area contained ~4.83 Mt of copper-mineralized rock. Using 0.5 wt.% Cu as the low-grade cut-off value and >0.8 wt.% Cu as the high-grade cut-off value, Hyvärinen (1966) estimated previously that the Virtasalmi mine area contained ~2 Mt of ore. Taking into consideration the open pit and underground production (Table 5), it can be shown that some 1.2 Mt of Cu-disseminated rock was left unmined. Approximately 650 000 tons of mineralized rock occur near the edges of the production pit and galleries and ~570 000

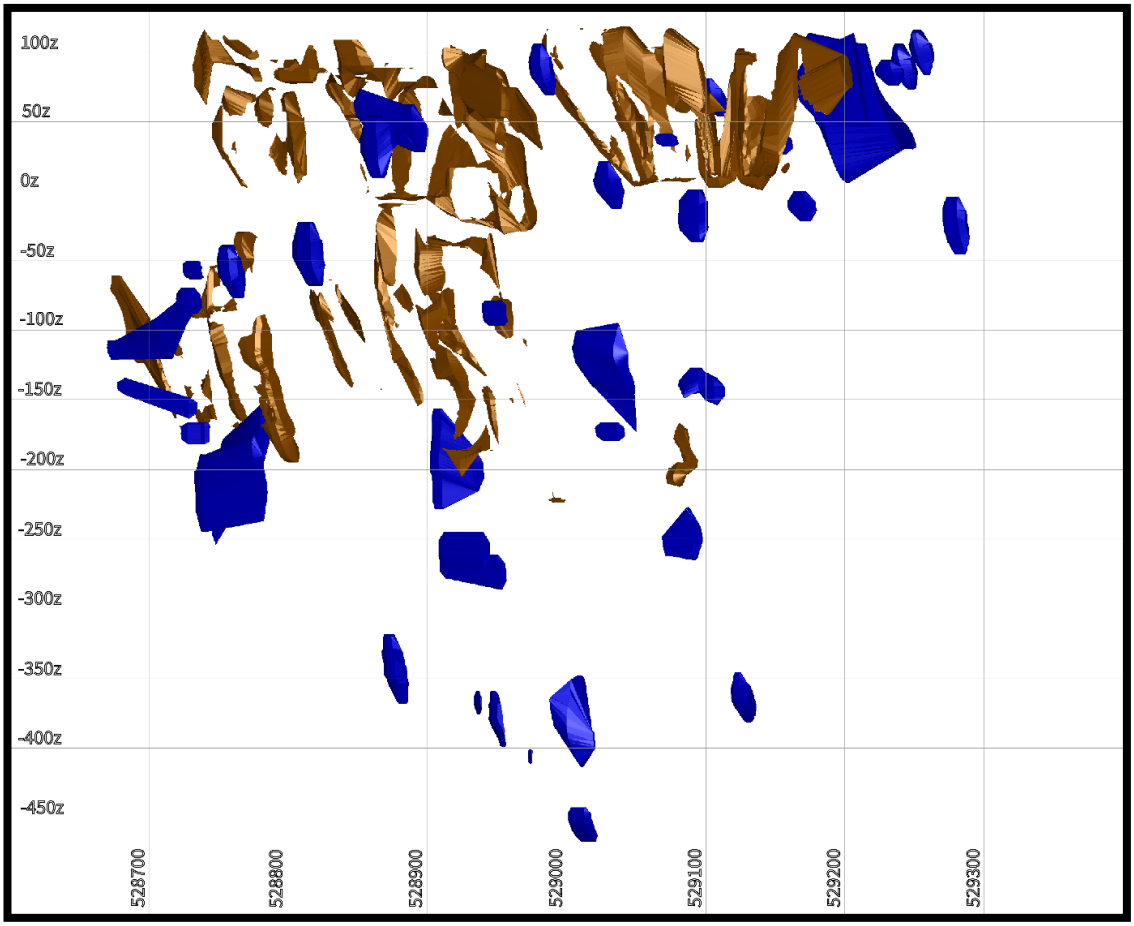

Fig. 24. Remaining mineralization solids after the production from the open pit and underground galleris has been subtracted. Brown solids are near the edges of the quarry and stopes. Blue solids are clearly outside the production areas. Looking north.

tons of mineralized rock is located clearly outside the production infrastructure. Outside the production areas of the mine, the mineralization is contained in unevenly distributed and variably sized lenses. These lenses are located on the extreme sides or underneath the main mineralization (Fig. 24).

8. Discussion

8.1 Coordinate and elevation system conversion

Even though the modeling and mapping software can be tweaked to work with custom coordinate grids and elevation systems, it was necessary to convert the collar database into the EUREFIN and N2000 systems so that the data can be added to the national GTK database. Conversion also causes further work and makes updates to the model easier since working with a custom grid makes mixing different data sources cumbersome. Especially, adding new, high-precision measurements would be difficult, if not impossible, without conversion, which would degrade the quality of the data.

Especially the coordinate system conversion proved to be very effective and accurate and could easily be implemented to a far larger dataset. A larger potential for errors is in the height data of the collar positions, which is caused partly by the original data being recorded in two different height systems and partly because the elevation data of the collars were eventually defaulted to a high-precision LIDAR topo-surface. This method leaves some uncertainty to the elevation position of the collars because of the LIDAR correction was applied in bulk and the underground collars had no reference point into which they could be tied to. Still the potential error is only up to ±2 meters and visual comparison between the reconstructed mine infrastructure and underground collar positions correlate well within the error limit.

8.2 Model validation

To test the accuracy of the model, tonnage estimation of the modeled mineralization bodies and the production stopes were calculated, and the results were compared with historical data obtained from unpublished Outokumpu Oy technical reports and third-party publications.

Comparison with the historical data shows good correlation between unified ore and waste production and would imply that the modeled open pit and production stopes are accurate (Table 6). However, the "true" ore production, especially from the underground stopes, initially lacked roughly 1 Mt of mineralized rock. The underground stope sizes had to be increased by 1.5 meters to accommodate more mineralized rock inside the stope solids and to make the modeled ore production fit better with the historical data (Table 6). Further stope optimization and more precise density data would likely account for the missing 0.3–0.46 Mt of estimated production.

It is a positive sign that the digitized mine has less production than its historical equivalent. Where drill core data were lacking, unoptimized underground stope solids were used as a guide for the mineralization shape and even though the stope-solids are, to a degree, too small, it has not affected the dimension of the overall mineralization. A substantial error source could have been the old hand-drawn mine maps, which were used for the digitalization and modeling of the production stopes. Errors in stope sizes could have occurred during the drawing of the original maps, during the digitalization process or during both simply by human error. The latest map with the drawing year stated is from 1971 but most of the underground level maps lack clear dates. Furthermore, there is no clear indication in the maps whether they are plans or actual representations of the finished stopes.

Table 5. Total volumes of Cu mineralization solids, open pit and underground galleries.

	Volume (m^3)
High-grade mineralization zone	314521
Low-grade mineralization zone	1237921
Open pit	505521
Underground galleries	974524
Optimized underground galleries	1285331

Table 6. Historical and modeled production estimates.

	Reported (Mt)	Modeled (Mt)	Diff. (Mt)
Open pit and underground stopes (ore and waste)	5.39 (OKU report)	5.04	0.35
Total mine production (ore)	4.3 (OKU report)	3.85	0.45
Total mine production (ore)	4.18 (Puustinen 2003)	3.85	0.33
Total mineralization estimation	~2 (Hyvärinen 1966)	4.83	2.83

8.3 Resource estimation

The overall mineralization estimation, which is presented in this study, of ~4.83 Mt copper (table 5), is a crude and unofficial estimation based only on historical data. Still it correlates well with the presently modeled and historically reported ore production of the Virtasalmi mine and additionally, is well over the initial ~2 Mt of ore estimated by Hyvärinen (1966). With a modeled total production of 3.85 Mt of ore, it means that estimated 1.2 Mt of mineralized material would have be left unmined after the closure of the Virtasalmi mine. However, this number is likely erroneous. Most of the ~650 000 tonnes of mineralized material near the underground stope edges (Fig. 24) could likely be removed by stope optimization. Assuming that the mine operators had more drill information at their disposal than in this study, it is unlikely that this amount of potential ore would have been left behind so close to the existing infrastructure. The mineralized material away from production areas which was left unmined accounts to roughly half a million tonnes of ore material and is scattered into lenses around the main mineralization. Most of the lenses are very small, far apart and would have been unfeasible to mine out. The estimated ~570 000 tonnes of mineralization in these separated lenses is likewise, prone to error since most of the lenses outside the main mineralization are based only on one or two drill core intersections (Figs. 20 and 21). While some of the intersections contain notable Cu grades associated with skarnified rocks, the size of these lenses could be anything from some meters to several tens of meters. Further drilling and modeling would be needed to ascertain the true amount of mineralized rock away from the production areas.

8.4 Comparison of the Virtasalmi mineralization with other similar deposits

In addition to the Cu sulfide-dominated mode of mineralization, the Virtasalmi deposit shares some features with some other Cu-rich VMS deposits, which range greatly in their age of formation (Corbett 2001, Appel 1997, Schiffman et al. 1987, Skirrow 1982). The disseminated VMS mineralization in the Isua area in western Greenland is, like the Virtasalmi deposit, hosted by banded tuffaceous amphibolites. In addition, the disseminated Cu mineralization at Isua occurs spatially close to iron formations which are possibly genetically connected with the disseminated sulfides (Appel 1997). This is also the case at Virtasalmi where Lawrie (1988) reported magnetite overtaking Cu sulfides distal to the main ore zones and hinted towards a genetic link.

The Troodos ophiolite in Cyprus hosts a Cu-dominated VMS deposit, which has been shown to have formed distal to a major spreading center. This deposit contains granular epidote-rich rocks underneath the feeder zone of the VMS system. A passive continental margin, a tectonic setting likely situated away from major spreading centers, was suggested by Lawrie (1992). Also, the "epidosites" identified in the Troodos deposit could be a lower metamorphic grade equivalents of the massive garnet rocks found at Virtasalmi (Lawrie 1988). The Mt. Lyell mining district in Tasmania hosts several VMS deposits, some of which include traditional massive VMS mounds. A few deposits at Mt. Lyell consist of Cu sulfide-dominated dissemination and veining. Corbett (2001) suggests that the Cu-disseminated areas used to have massive sulfide mounds stratigraphically above them, but later erosion has destroyed the deposits. The situation could be similar at Virtasalmi where chalcopyrite dominates the mineralization and the system lacks clear massive sulfide lenses (Lawrie 1988).

8.5 Further research

It could be beneficial to structurally relog some or all of the remaining drill cores from the Virtasalmi mine. Structural observations made from the drill cores during exploration and operation of the mine have been sparse and while these data were digitized for this thesis, the amount of the data points is far too small to be useful in 3D analysis. Shear zones with a "large" but uncertain amount of movement have been

recorded in the mine area (Hyvärinen 1966, Lawrie 1988), Better structural information could be a key in finding deeper parts of the mineralization.

Whole-rock geochemistry from the Virtasalmi rocks has not been obtained or, if existent, the data are missing. Re-analysis of the remaining drill cores could provide further information about the alteration halos proximal and distal to the high-grade garnet skarn zones. Deeper understanding on how the alteration envelopes behave near the mineralization would be very useful if further drilling underneath or near the Virtasalmi mineralization is to be conducted.

Based on unpublished Outokumpu Oy records, the mine was commonly struggling to meet production goals and suffered from over-estimation of ore grades. Re-analysis for copper should be conducted on old drill cores and comparison to the historical data conducted to pin-point possible errors in the historical dataset. Additionally, the drill core dataset has not yet been analyzed for gold even though gold is a common element in VMS systems and one of the first exploration holes (R3) showed weak indications of gold and silver, but the contemporary workers did not identify the Virtasalmi deposit as an example of VMS mineralization.

9. Conclusions

1. According to the model developed in this work, there was ~4.83 Mt of copper ore in the Virtasalmi mine area before the mining operations were started. After the production ceased, roughly 500 000 tons of ore is estimated to have remained unmined.

2. High-grade and low-grade mineralization is most abundant near the surface in the mineralization lens A. With depth, the mineralized lenses become thinner and eventually break into small singular lenses under the main mineralization lenses.

3. Lenses with high copper grades are associated with the proximity of garnet skarns.

4. Despite the shortcomings of the historical data and the human factor in drawing and digitalization, the modeled mine infrastructure can be regarded as a good representation of the real life mine at Virtasalmi. The unoptimized underground stopes provide a relatively accurate starting point for further stope optimization if more historical reference material should become available.

Acknowledgements

I would like to thank the Geological Survey of Finland for providing me access to the historical data used and presented in this study and University of Oulu for providing access to the software needed for data manipulation. I would like to thank Janne Hokka from GTK for his invaluable guidance on the subject, principles of 3D-modeling and for the opportunity to see some rocks from the Virtasalmi mine. Sincere thanks to Marko Moilanen for helping me in getting started with SURPAC and for helpful tips on the thesis, to Holger Paulick for review and suggestions on corrections and for Prof. Eero Hanski for helping me to cross the finish line. Also, I must express my warmest gratitude towards the good people of honorofboys.club for company during many a long nights of work. Finally, thousands of thanks to my wife Anne for sharing her thoughts on the subject and for infinite support and encouragement during the thesis project.

References

Appel, P. 1979. Stratabound copper sulfides in a banded iron-formation and in basaltic tuffs in the early Precambrian Isua supracrustal belt, West Greenland. Economic Geology 74, 45-52.

Arndt, N.T., Briigmann, G.E., Lehnert, K., Chauvel, C., Chappell, B.W. 1987. In: T.C. Pharaoh, R.D. Beckinsale and D. Rickard (Eds.) Geochemistry and Mineralization of the Proterozoic Volcanic Suites. Geological Society, Special Publication 33, 133-145.

Barager, W.R., Scoates, R.F.J. 1987. Volcanic geochemistry of the northern segments of the Circum-Superior Belt of the Canadian Shield. In: T.C. Pharaoh, R.D. Beckinsale and D. Rickard (Eds.) Geochemistry and Mineralization of the Proterozoic Volcanic Suites. Geological Society, Special Publication 33, 113-131.

Bonnet, A.-L., Corriveau, L. 2007. Alteration vectors to metamorphosed hydrothermal systems in gneissic terranes. In: Goodfellow, W.D. (Ed.) Mineral deposits of Canada - A synthesis of major deposit-types, district metallogeny, the evolution of geological provinces, and exploration methods. Geological Association of Canada, Mineral Deposits Division, Special Publication 5, 1035–1049.

Bradley, D.C. 2011. Secular trends in the geologic record and the supercontinent cycle. Earth-Science Reviews 108, 16-33.

Cawood, P.A., Hawkesworth C.J. 2013. Temporal relations between mineral deposits and global tectonic cycles. Geological Society of London, Special Publications 393, 9-21.

Corbett, K.D. 2001. The geology of The Mount Lyell mines area, Tasmania – a re-interpretation based on studies at Lyell Comstock, North Lyell and The Iron Blow area. Master's thesis, University of Tasmania, department of earth sciences. 116 p. Retrieved from: https://eprints.utas.edu.au/19127/

Galley, A.G., Hannington, M.D., Jonasson, I.R. 2007. Volcanogenic massive sulfide deposits. In: W.D. Goodfellow (Ed.) Mineral Deposits of Canada: A Synthesis of Major Deposit-Types, District Metallogeny, the Evolution of Geological Provinces, and Exploration Methods. Geological Association of Canada, Special publication 5, 141-161.

Groves, D.I., Vielreicher, R.M., Goldfarb, R.J., Condie, K.C. 2005. Controls on the heterogeneous distribution of mineral deposits through time. Geological Society of London, Special Publications 248, 71-101.

Hannington, M.D., Galley, A.G., Herzig, P.M., Petersen, S. 1998. Comparison of the TAG mound and stockwork complex with Cyprus-type massive sulfide deposits; Proceedings of the Ocean Drilling Program. Scientific Results 158, College Station, TX, 389-415.

Hanski, E. 2015. Synthesis of the geological evolution and metallogeny of Finland. In: Maier, W.D., Lahtinen, R., O'Brien H. (Eds.) Mineral deposits of Finland, Elsevier, Amsterdam, p. 507-530.

Herzig, P.M., Hannington, M.D. 1995. Polymetallic massive sulfides at the modern seafloor: A review. Ore Geology Reviews 10, 95-115.

Hokka, J., Virnes, L. 2017. Lithogeochemical pXRF study on the Virtasalmi Cu deposit, Eastern Finland. Manuscript submitted for publication.

Huhma, H. 1986. Sm-Nd, U-Pb and Pb-Pb isotopic evidence for the origin of the Early Proterozoic Svecokarelian crust in Finland. Geological Survey of Finland, Bulletin 337, 48 p.

Humphris, S.E. and 24 others 1995b. The internal structure of an active seafloor massive sulfide deposit. Nature 377, 713-716.

Huston, D.L., Brauhart, C.W., Drieberg, S.L., Davidson, G.J., Groves, D.I. 2001. Metal leaching and inorganic sulfate reduction in volcanic-hosted massive sulfide mineral systems: Evidence from the paleo-Archean Panorama district, Western Australia. Geology 29, 687-690.

Huston, D.L., Large, R.R. 1989. A chemical model for the concentration of gold in volcanogenic massive sulfide deposits. Ore Geology Reviews 4, 171-200.

Huston, D.L., Pehrsson, S., Eglington, B.M., Zaw, K. 2010. The geology and metallogeny of volcanic-hosted massive sulfide deposits: variations through geologic time and with tectonic setting. Economic Geology 105, 571-591.

Hyvärinen, L. 1966. Karsikummun kupariesiintymän geologiasta. Geological Survey of Finland. Unpublished report M17/Vrs-/66/1 (in Finnish).

Hyvärinen, L. 1969. On the geology of the copper ore field in the Virtasalmi area, eastern Finland. Geological survey of Finland, Bulletin 240, 87 p.

Hölttä, P. 1995. Contact metamorphism of the Vaaraslahti pyroxene granitoid intrusion in Pielavesi, central Finland. In: P. Hölttä (Ed.) Relationship of granitoids, structures and metamorphism at the eastern margin of the Central Finland Granitoid Complex. Geological Survey of Finland. Bulletin 382, 27-79.

Hölttä, P. 1988. Metamorphic zones and the evolution of granulite grade metamorphism in the early Proterozoic Pielavesi area, central Finland. Geological Survey of Finland. Bulletin 344, 1-50.

Jansson, N., Hermansson, T., Fjellerad Persson, M., Berglund, A., Kruuna, A., Skyttä, P., Bachmann, K., Gutzmer, J., Chmielowski, R.M., Weihed, P. 2013. Recent advances in structural geology, lithogeochemistry and exploration for VHMS deposits, Kristineberg area, Skellefte District, Sweden. In: 12th Biennial SGA Meeting: Mineral deposit research for a high-tech world. Uppsala, Sweden 12/08/2013-15/08/2013, 545-548.

Kerrich, R., Goldfarb, R.J., Richards J. 2005. Metallogenic provinces in an evolving geodynamic framework. Economic Geology 100th Anniversary Volume, 1097-1136.

Kontinen, A., Peltonen, P., Huhma, H. 2006. Description and genetic modelling of the Outokumpu-type rock assemblage and associated sulfide deposits. GTK report M 10.4/2006/1.

Korsman, K., Koistinen, T., Kohonen, J., Wennerström, M., Ekdahl, E., Honkamo, M., Idman, H., Pekkala, Y. (Eds.) 1997. Bedrock map of Finland 1:1 000 000. Espoo. Geological Survey of Finland.

Korsman, K., Korja, T., Pajunen, M., Virransalo, P., and GGT/SVEKA Working Group. 1999. The GGT/SVEKA Transect: Structure and Evolution of the Continental Crust in the Paleoproterozoic Svecofennian Orogen in Finland. International Geology Review 41, 287-333.

Koski, R.A., Mosier, D.L. 2012. Deposit type and associated commodities in volcanogenic massive sulfide occurrence model. U.S. Geological Survey Scientific Investigations. Report 2010–5070 –C. Chap. 2. pp. 8.

Kousa, J., Marttila, E., Vaasjoki, M. 1994. Petrology, geochemistry and dating of Paleo proterozoic metavolcanic rocks in the Pyhäjärvi area, central Finland. In: M. Nironen, Y. Kähkönen (Eds.) Geochemistry of Proterozoic supracrustal rocks in Finland. Geological Survey of Finland, Special Paper 19, 7-27.

Kähkönen, Y. 2005. Svecofennian supracrustal rocks. In: M. Lehtinen, P.A. Nurmi and O.T. Rämö (Eds.) Precambrian Geology of Finland – Key to the Evolution of the Fennoscandian Shield. Elsevier, Amsterdam, p. 343 – 406.

Kärki, A., Laajoki, K. 1995. An interlinked system of fold and ductile shear zones – late stage Svecokarelian deformation in the central Fennoscandian Shield, Finland. Journal of Structural Geology 17 (9), 1233 – 1247.

Lawrie, K.C. 1992. Geochemical characterisation of a polyphase, deformed, altered and high grade metamorphosed volcanic terrane: implications for the tectonic setting of the Svecofennides, south-central Finland. Precamprian Research 59, 171 – 205.

Lawrie, K.C. 1988. The origin, nature and tectonic significance of the Hällinmäki copper deposit, south-central Finland. Unpub. PhD thesis. Glasgow University.

Lewry, J.F., Macdonald, R., Livesy, C., Meyer, M., Van Schmus, R., Bickford, M.E. 1987. U-Pb geochronology of accreted terranes in the Trans-Hudson Orogen, Northern

Saskatchewan, Canada. In: T.C. Pharaoh, R.D. Beckinsale and D. Rickard (Eds.) Geochemistry and Mineralization of the ProterozoicVolcanic Suites. Geological Society. Special Publication 33, 147-166.

Li, X., Yuan, F., Zhang, M., Jia, C., Jowitt, S., Ord, A., Zheng, T., Hu, X., Li, Y. 2015. Three-dimensional mineral prospectivity modelling for targeting of concealed mineralizations within the Zhonggu iron orefield, Ningwu Basin, China. Ore Geology Reviews 71, 633-654.

Lydon, J.W. 1988. Ore deposit models #14. Volcanogenic massive sulfide deposits Part 2: Genetic models. Geoscience Canada 15 (1), 43-65.

Martin, L., Perron, G., Masson, M. 2007. Discovery from 3D Visualization and Quantitative Modelling. In B. Milkereit (Ed.) Proceedings of Exploration 07: Fifth Decennial International Conference on Mineral Exploration, 543-550.

Nironen, M. 1989. Emplacement and structural setting of granitoids in the early proterozoic Tampere and Savo schist belts, Finland - Implications for contrasting crustal evolution. Geological Survey of Finland, Bulletin 346, 83 p.

Pekkarinen, L. 2002. Haukivuoren ja Pieksämäen kartta-alueiden kallioperä. Summary: Pre-Quaternary rocks of the Haukivuori and Pieksämäki map-sheet areas. Kallioperäkartan selitys 1:100 000 - Expl. to Maps of Pre-Quat. Rocks, sheets 3231 and 3232. Geological survey of Finland, 98 p.

Peltonen, P., Kontinen, A., Huhma, H., Kuronen, U., 2008. Outokumpu revisited: New mineral deposit model for the mantle peridotite-associated Cu-Co-Zn-Ni-Ag-Au sulphide deposits. Ore Geology Reviews 33, 559–617.

Perkins, C., Walshe, J.L. 1993. Geochronology of the Mount Read Volcanics, Tasmania, Australia. Economic Geology 88, 1176-1197.

Peter, J.M., Scott, S.D. 1988. Mineralogy, composition, and fluid-inclusion microthermometry of seafloor hydrothermal deposits in the southern trough of Guaymas Basin, Gulf of California. Canadian Mineralogist 26, 567-587.

Pisutha-Arnond, V., Ohmoto, H. 1983. Thermal history and chemical and isotopic compositions of ore-forming fluids responsible for kuroko massive sulfide deposits in the Hokoruku district of Japan. Economic Geology Monograph 5, 523-558.

Puustinen, K. 2003. Suomen kaivosteollisuus ja mineraalisten raaka-aineiden tuotanto vuosina 1530–2001, historiallinen katsaus erityisesti tuotantolukujen valossa. Geological Survey of Finland. M10.1/2003/3 (in Finnish).

Raymond, O.L. 1996. Pyrite composition and ore genesis in the Prince Lyell copper deposit, Mt Lyell mineral field, western Tasmania, Australia. Ore Geology Reviews 10, 231-250.

Reinikainen, J. 2001. Petrogenesis of Paleoproterozoic marbles in the Svecofennian Domain, Finland. Geological Survey of Finland, Report of Investigation 154, 84 p.

Rona, P.A. 1980. TAG hydrothermal field: Mid-Atlantic Ridge crest at latitude 268N. J. Geological Society of London 137, 385-402.

Rona, P.A. 1984. Hydrothermal mineralization at sea floor spreading centers. Earth-Science Reviews 20, 1-104.

Shanks III, P.W.C., Koski, R.A. 2012. Volcanogenic massive sulfide occurrence model U.S. Geological Survey Scientific Investigations Report 2010–5070–C. chap. 1. p. 4.

Shirozu, H. 1974. Clay minerals in altered wall rocks of the kuroko-type deposits. Mining Geology Special Issue 6, 303-311.

Skirrow, R. 1982. Origin of sulphur and geothermometry of hydrothermal sulfides from the Galapagos Rift, 86 °W. Nature 299, 142-144.

Solomon, M. 1976. "Volcanic" massive sulfide deposits and their host rocks - a review and explanation. In: Wolf K. (Ed.). Handbook of Stratabound and Stratiform Ore Deposits. Elsevier, Amsterdam, p. 21-54.

Thompson, G., Humphris, S.E., Schroeder, B., Sulanowska, M., Rona, P.A. 1988. Active vents and massive sulfides at 268N (TAG) and 238N (Snakepit) on the Mid-Atlantic-Ridge. Canadian Mineralogist 26, 697-711.

Vaasjoki, M., Sakko, M. 1988. The U-Pb mineral chronology of the Raahe-Ladoga zone. In: Pajunen, M. (Ed.) Project No. 235 “Metamorphism and geodynamics” excursion in Finland 15.6.-19.6.1988. Geological Survey of Finland, Guide 21, 23-24.

Van Kranendonk, M.J., Hickman, A.H., Smithies, R.H., Williams, I.R., Bagas, L., Farrell, T.R. 2006a. Revised lithostratigraphy of Archean supracrustal and intrusive

rocks in the northern Pilbara Craton, Western Australia. Western Australia Geological Survey Record 2006/15. 57 p.

Väisänen, M., Mänttäri, I., Kriegsman, L.M., Hölttä, P. 2000. Tectonic setting of post-collisional magmatism in the Palaeoproterozoic Svecofennian Orogen, SW Finland. Lithos 54 (1-2), 63-81.

Walshe, J.L., Solomon, M. 1981. An investigation into the environment of formation of the volcanic-hosted Mt Lyell copper deposits using geology, mineralogy, stable isotopes and a six-component chlorite solid solution model. Economic Geology 76, 246-284.

Yang, F., Wang, G., Santosh, M., Li, R., Tang, L., Cao, H., Guo, N., Liu, C. 2017. Delineation of potential exploration targets based on 3D geological modelling: A case study from the Laoangou Pb-Zn-Ag polymetallic ore deposit, China. Ore Geology Reviews 89, 228-252.

Yang, K., Scott, S.D. 1996. Possible contribution of a metal-rich magmatic fluid to a seafloor hydrothermal system. Nature 383, 420-423.

Appendix: Drill hole information

Hole ID	Easting (EUREFIN)	Northing	Collar Depth Meters	Collar azimuth Degrees	Collar dip Degrees	LENGTH Meters	YEAR
HM1	528832	6880768	101.8	270	-46	35.3	
HM2	528843	6880761	102.3	270	-31	35.3	
HM3	528852	6880752	102.2	270	-42	36.2	
HM4	528871	6880736	103.0	270	-31	45.1	
HM5	528881	6880728	103.0	270	-35	45.1	
HM6	528904	6880714	105.5	270	-35	46.5	
HM7	528914	6880707	106.6	270	-40	45.3	
HM8	528924	6880699	108.0	270	-41	45.3	
HM9	528811	6880748	112.6	270	-19	43.4	
HM10	528854	6880720	112.0	90	-19	23.7	
HM11	528891	6880685	111.4	270	-37	13.4	
HM12	528898	6880676	111.0	270	-42	13.4	
HM13	528914	6880673	111.5	270	-35	20.0	
HM14	528877	6880741	102.4	270	-55	28.4	
HM15	528887	6880733	103.2	270	-54	29.4	
HM19	529135	6880539	42.9	45	-27	50.6	
HM20	529136	6880539	42.8	136	-27	62.0	
HM21	529135	6880540	42.8	17	-18	63.5	
HM31	528848	6880728	-13.5	45	-33	51.6	1973
HM32	528846	6880726	-14.8	225	-45	55.6	1973
HM33	528900	6880695	-37.8	45	0	45.7	1973
HM36	528810	6880713	-46.1	225	-10	86.1	1973
HM37	528810	6880713	-46.7	45	-42	120.3	1973
HM40	528808	6880746	-65.9	45	21	32.5	1974
HM41	528808	6880746	-67.3	45	-30	70.2	1974
HM42	528851	6880732	-69.0	45	18	48.3	1974
HM43	528899	6880694	-75.6	45	-16	45.5	1974
HM44	528886	6880714	-73.8	45	0	40.3	
HM45	528886	6880714	-74.7	45	-53	111.0	1974
HM46	528899	6880694	-76.3	45	-58	125.3	1974
HM47	528915	6880675	-79.2	45	-43	80.6	1974
HM48	528948	6880637	-84.3	45	-19	91.1	1974
HM49	528948	6880637	-84.6	45	-36	115.1	1974
HM50	528981	6880599	-90.0	45	-34	114.7	1974
HM51	528932	6880656	-81.7	45	-25	65.2	1974
HM52	528965	6880618	-87.3	45	-46	126.1	1974
HM53	528932	6880656	-82.0	45	-50	118.1	1974
HM54	529010	6880592	-94.3	45	-44	123.0	1974
HM55	528946	6880703	-1.1	45	0	41.0	1974
HM56	529010	6880592	-93.9	45	-26	90.3	
HM57	529035	6880581	-95.5	45	-48	135.5	1975

Hole ID	Easting (EUREFIN)	Northing	Collar Depth Meters	Collar azimuth Degrees	Collar dip Degrees	LENGTH Meters	YEAR
HM58	529035	6880581	-95.2	45	-20	85.6	1975
HM59	529248	6880498	24.1	45	-54	139.7	1976
HM60	528932	6880656	-79.4	45	45	120.1	1975
HM61	529248	6880498	24.1	45	-73	174.3	1975
HM62	529179	6880524	15.8	45	-45	140.6	1976
HM63	529250	6880496	24.2	80	-40	131.7	1975
HM64	529009	6880592	-94.4	45	-70	181.5	
HM65	529009	6880592	-94.4	45	-62	160.3	1975
HM66	528851	6880731	-114.3	45	-15	85.3	1975
HM67	528834	6880735	-117.1	45	-35	89.5	1976
HM68	528762	6880771	-129.9	45	0	65.7	1976
HM69	528775	6880750	-126.6	45	-37	85.6	1976
HM70	528805	6880743	-121.1	45	-16	96.6	1976
HM71	528754	6880780	-130.7	354	0	70.3	1976
HM72	528762	6880771	-130.9	45	-48	94.0	1976
HM73	528762	6880771	-128.4	45	45	47.5	1976
HM74	528710	6880759	-128.6	1	0	106.8	1976
HM75	528711	6880758	-127.7	45	30	83.8	1976
HM76	528711	6880758	-129.0	45	-23	120.6	1976
HM77	528762	6880771	-130.2	45	-27	52.1	1976
HM78	528750	6880763	-58.1	45	0	45.8	1976
HM79	528749	6880764	-58.1	358	0	59.1	1976
HM80	528750	6880763	-56.9	45	42	40.1	1976
HM81	528750	6880763	-59.0	45	-32	45.6	1976
HM82	528883	6880713	-149.6	45	28	65.6	1976
HM159	529172	6880709	-216.1	263	-61	328.4	1982
HM158	529171	6880707	-216.1	199	-52	249.3	1982
HM157	529171	6880707	-216.1	198	-23	177.5	1982
HM156	529172	6880709	-216.2	231	-55	281.5	1982
HM155	528982	6880635	-211.4	45	-60	151.9	1982
HM154	528950	6880639	64.7	45	-27	101.1	1982
HM153	529061	6880640	-218.2	225	-76	140.2	1982
HM152	528770	6880666	-191.4	253	-49	348.6	1981
HM151	528764	6880670	-191.1	50	-48	349.2	1981
HM150	528767	6880665	-191.3	90	-43	404.3	1981
HM149	528762	6880671	-191.1	3	-47	348.9	1981
HM147	529032	6880627	-96.7	13	0	43.6	1981
HM146	529032	6880628	-97.5	13	-35	55.6	1981
HM145	528723	6880837	-164.3	225	-23	67.0	1981
HM144	528939	6880663	-202.1	45	-47	138.6	
HM143	529036	6880581	-94.9	72	-30	82.0	
HM142	529011	6880610	-168.3	45	7	76.2	
HM141	528900	6880690	-196.0	45	-51	113.5	
HM140	529030	6880594	-168.6	45	0	70.6	

Hole ID	Easting (EUREFIN)	Northing	Collar Depth Meters	Collar azimuth Degrees	Collar dip Degrees	LENGTH Meters	YEAR
HM139	528640	6880828	-126.1	45	-52	171.0	1980
HM138	528711	6880758	-129.7	45	-52	166.0	
HM137	528676	6880793	-127.4	45	-54	164.9	
HM136	528675	6880793	-127.2	45	-44	154.6	
HM135	528874	6880739	-188.7	45	-57	110.2	1979
HM134	528875	6880739	-187.5	45	-35	68.1	1979
HM133	528875	6880739	-186.5	23	0	51.0	1979
HM132	529021	6880602	-170.0	45	-55	130.9	1979
HM131	529038	6880585	-168.7	45	-51	134.0	
HM130	529013	6880629	-170.9	45	-57	120.5	1978
HM129	528895	6880758	-106.6	225	-48	43.9	1978
HM128	528875	6880739	-186.5	45	0	53.2	1978
HM127	528874	6880739	-185.9	45	25	53.9	1978
HM126	528761	6880804	-166.1	45	-40	53.2	1978
HM125	528917	6880744	-181.2	45	58	37.2	1978
HM124	528746	6880765	-58.2	342	0	69.4	1978
HM123	528931	6880723	-182.7	45	-21	44.7	1978
HM122	528931	6880723	-181.2	45	30	48.8	1978
HM121	528965	6880687	-178.9	45	-20	40.1	1978
HM120	528965	6880686	-177.3	45	40	29.0	1978
HM119	528985	6880671	-175.9	45	-32	40.8	1978
HM118	528985	6880671	-174.5	45	30	31.4	1978
HM117	528943	6880666	-157.0	45	30	57.1	1978
HM116	529036	6880582	-168.2	225	-35	60.3	
HM115	529040	6880584	-167.4	50	0	90.5	1978
HM114	529039	6880585	-167.8	45	-15	76.9	1978
HM113	529039	6880585	-166.5	45	35	66.7	1978
HM112	529021	6880603	-167.4	45	20	70.0	1978
HM111	529014	6880630	-170.4	45	-23	67.6	1978
HM110	528676	6880793	-125.3	45	16	86.2	1978
HM109	528693	6880775	-125.6	45	44	84.3	1978
HM108	528693	6880775	-126.4	45	12	81.2	
HM107	528693	6880775	-126.9	45	-16	104.2	1977
HM106	528984	6880670	-173.7	45	0	66.9	1977
HM105	528640	6880828	-123.0	45	45	103.0	1977
HM104	529021	6880603	-168.1	45	-14	79.9	1977
HM103	528640	6880828	-124.9	45	-30	117.5	1977
HM102	528640	6880828	-123.7	45	10	84.8	1977
HM101	528910	6880704	-151.1	45	35	52.5	1977
HM100	528675	6880792	-124.3	45	60	79.7	1977
HM99	529006	6880657	-173.2	45	-45	91.0	1977
HM98	529039	6880585	-168.0	45	-33	109.9	1977
HM97	529039	6880585	-167.0	45	10	78.1	1977
HM96	529006	6880657	-171.5	45	30	51.5	1977

Hole ID	Easting (EUREFIN)	Northing	Collar Depth Meters	Collar azimuth Degrees	Collar dip Degrees	LENGTH Meters	YEAR
HM95	528656	6880812	-123.4	45	47	80.4	1977
HM94	528656	6880812	-125.5	45	-20	120.3	1977
HM93	528656	6880812	-124.3	45	20	73.4	1977
HM92	529013	6880629	-170.9	45	-46	99.3	1977
HM91	529013	6880630	-170.1	41	0	71.5	1977
HM90	528956	6880644	-162.8	45	-35	124.7	1977
HM89	528943	6880666	-158.9	45	-45	115.2	
HM88	528676	6880793	-126.9	45	-26	121.4	1977
HM87	528676	6880793	-125.2	45	35	79.8	1977
HM86	528930	6880688	-154.6	45	-20	67.2	
HM85	528674	6880794	-127.3	0	0	109.3	1977
HM84	528833	6880735	-117.4	45	-55	151.7	
HM83	528884	6880713	-151.5	45	-40	115.3	1976
HM16	528958	6880646	66.0	45	-4	91.5	
HM17	528891	6880652	71.0	270	-20	66.2	
HM22	529145	6880581	101.0	90	0	15.8	
HM23	529103	6880610	100.0	90	0	25.9	
HM24	529099	6880606	100.0	270	0	27.9	
HM26	529050	6880630	100.0	270	0	15.5	
HM27	528927	6880685	-4.3	45	-57	72.1	1973
HM28	528926	6880685	-3.9	45	-29	55.8	1973
HM29	528878	6880708	-10.3	45	-55	66.7	1973
HM30	528878	6880708	-9.4	45	-17	55.6	1973
HM34	528900	6880694	-36.9	45	23	61.5	1973
HM35	528900	6880694	-38.7	45	-32	50.6	1973
HM38	528866	6880745	-2.1	45	-47	24.6	1974
HM39	528866	6880745	-0.3	45	33	40.6	1974
R10	528831	6881005	119.1	225	-45	47.8	1965
R11	529098	6880641	118.3	225	-45	79.0	1965
R12	528979	6880801	119.2	225	-45	152.6	1965
R13	528838	6880772	118.3	225	-45	153.8	1964
R14	528819	6880791	118.3	225	-45	100.8	1964
R15	528943	6880699	118.3	225	-45	177.6	1965
R16	529003	6880821	119.3	225	-60	250.1	1965
R17	528872	6880839	118.3	225	-45	211.0	1965
R18	528955	6880827	118.7	225	-45	217.5	1965
R19	529010	6880763	120.2	225	-45	201.5	1965
R20	528926	6880856	118.3	225	-45	266.9	1965
R21	529037	6880788	119.9	225	-60	241.1	1965
R22	528984	6880855	119.0	225	-60	295.4	1965
R23	529086	6880758	120.6	225	-45	279.8	
R24	528966	6880838	118.8	225	-54	261.1	1965
R25	528947	6880877	118.7	225	-60	306.7	1965
R27	528931	6880893	118.3	225	-60	319.1	1965

Hole ID	Easting (EUREFIN)	Northing	Collar Depth Meters	Collar azimuth Degrees	Collar dip Degrees	LENGTH Meters	YEAR
R28	528967	6880839	118.8	225	-60	246.9	1965
R29	528906	6880736	118.3	225	-45	169.0	1965
R3	528878	6880756	118.3	225	-45	137.2	1964
R32	529015	6880947	119.7	225	-65	445.8	1965
R33	528996	6880927	119.6	225	-60	201.6	1965
R34	529049	6880916	120.1	225	-65	446.0	1965
R35	528786	6880828	121.3	225	-45	154.5	1965
R36	528981	6880941	118.8	225	-63	411.1	1965
R37	529052	6880870	119.9	225	-63	345.5	1965
R38	528816	6880797	118.3	225	-45	151.5	1965
R39	528893	6880822	118.3	225	-40	171.4	1965
R4	528912	6880788	118.5	225	-45	109.6	1964
R40	528819	6880772	118.3	225	-30	83.2	1965
R41	528716	6880896	119.6	225	-42	140.0	1965
R42	528831	6880766	118.3	225	-30	80.4	1965
R43	529011	6880687	118.6	225	-45	71.5	1965
R44	529042	6880655	118.3	225	-45	83.2	1965
R45	529143	6880683	121.1	225	-45	157.8	1965
R46	529188	6880658	120.4	225	-45	157.1	1965
R47	529259	6880585	122.6	225	-30	109.2	1965
R48	529087	6880834	120.4	225	-63	378.1	1965
R49	528909	6880873	118.3	225	-55	260.7	1965
R5	529032	6880707	120.2	225	-45	112.8	1964
R51	529110	6880855	120.7	225	-67	453.6	1965
R52	528843	6880761	118.3	225	-45	106.2	1965
R53	528854	6880754	118.3	225	-30	90.6	1965
R54	528864	6880746	118.3	225	-30	74.1	1965
R55	528875	6880739	118.3	225	-30	67.6	1965
R56	528885	6880732	118.3	225	-30	65.6	1965
R57	528895	6880724	118.3	225	-30	65.6	1965
R58	528907	6880717	118.3	225	-30	64.4	1965
R59	528917	6880709	118.3	225	-30	66.3	1965
R6	529033	6880708	120.4	225	-90	150.9	1964
R60	528808	6880779	118.3	225	-30	66.2	1965
R61	529062	6880810	120.2	225	-62	307.6	1965
R62	529145	6880820	121.3	225	-65	383.8	1965
R63	529141	6880614	116.0	225	-30	114.1	1965
R64	529185	6880583	115.3	225	-45	101.9	1965
R65	528909	6880739	118.3	225	-90	321.4	1965
R66	529226	6880622	121.0	225	-45	140.3	1965
R67	529225	6880691	121.3	225	-46	194.4	1965
R68	529108	6880716	121.2	225	-45	189.2	1965
R69	529123	6880799	121.0	225	-63	354.6	1965
R7	528984	6880738	121.0	225	-45	263.9	1964

Hole ID	Easting (EUREFIN)	Northing	Collar Depth Meters	Collar azimuth Degrees	Collar dip Degrees	LENGTH Meters	YEAR
R70	529181	6880786	121.3	225	-65	413.9	1966
R71	529195	6880731	121.3	225	-63	330.9	1965
R72	529286	6880678	121.3	225	-63	351.2	1966
R73	529296	6880621	122.9	225	-50	229.8	1965
R74	528797	6880786	118.3	225	-30	63.5	1965
R75	529223	6880829	119.6	225	-67	649.0	1965
R76	529265	6880658	121.3	225	-50	329.9	1965
R77	528787	6880793	118.6	225	-30	58.5	1965
R78	528775	6880799	121.3	225	-30	70.0	1965
R79	528763	6880806	121.3	225	-30	56.7	1965
R8	528934	6880761	119.8	225	-45	110.7	1965
R80	529168	6880705	121.3	225	-60	383.8	1965
R82	529150	6880756	121.3	225	-55	346.5	1966
R83	529330	6880515	121.4	225	-45	122.5	1965
R84	529014	6880724	121.3	225	-30	218.7	1966
R85	529220	6880548	115.3	225	-45	71.9	1965
R86	528927	6880702	118.3	225	-30	67.1	1965
R87	528939	6880695	118.3	225	-30	71.3	1965
R88	529226	6880693	121.3	225	-58	258.2	1966
R89	528848	6880781	118.3	225	-45	129.2	1966
R9	529062	6880676	119.2	225	-45	79.7	1965
R70A	529181	6880786	-31.0	225	-65	235.0	1966